KHAN, SAFEERA, M.S. Carbon Nanodots in Endothelial Cells and C57BL/6 Mice: A Study of Toxicity and Anti-inflammatory Effect. (2018).
Directed by Dr. Zhenquan Jia. 55 pp.

The advancement of therapy for cardiovascular disease (CVD) is paramount to public health, as it is the leading global cause of mortality [1]. Nanomedicine provides new opportunities in the ongoing efforts to reduce the economic and healthcare consequences of CVD. Carbon Nanodots (CNDs) green-synthesized from microwave pyrolysis of ethylenediamine and citric acid are spherical, ~3 nm in diameter, and possess exceptional hydrophilic, biocompatible, fluorescent, and anti-oxidant properties. However, there is no current report on how these CNDs affect the cardiovascular system, particularly their potential in mediating endothelial dysfunction and cardiovascular disease (CVD). As a known biomarker of inflammation, Oxidized-LDL (Ox-LDL) induces inflammatory gene expression and monocyte extravasation that leads to atherosclerotic development. This study examines the role of CNDs in mediating Ox-LDL induced inflammation in human microvascular endothelial cells (HMEC-1). Our results demonstrate that CNDs can reduce Ox-LDL induced monocyte adhesion in HMEC-1s, which demonstrates their anti-inflammatory effects. The relative gene expression of the cytokine interleukin-8 (IL-8) was reduced by the addition of CNDs, which implies their action in mediating monocyte recruitment to the site of inflammation. While reactive oxygen species (ROS) perform many essential functions, their overproduction disrupts cellular oxidative balance, induces EC dysfunction, and leads to an inflammatory state. Studying the action of CNDs through Electron paramagnetic resonance (EPR) spectroscopy showed direct superoxide and hydroxyl radical-

scavenging by CNDs. This result implies that the anti-inflammatory effects of CNDs seen in vitro are attributed to their direct scavenging of ROS. Furthermore, CNDs were found to ameliorate the cytotoxicity caused by Ox-LDL in HMEC-1s. Viability assays showed CNDs were not cytotoxic at measured concentrations to HMEC-1s in vitro. Animal studies involving mice did not show any morphological or physical changes between the CND and control groups. These collective results demonstrate the potential of CNDs to reduce inflammation and cytotoxicity caused by Ox-LDL in HMEC-1s, which implies their use in the development of novel therapy for cardiovascular disease.

CARBON NANODOTS IN ENDOTHELIAL CELLS AND C57BL/6 MICE:

A STUDY OF TOXICITY AND ANTI-INFLAMMATORY EFFECT

by

Safeera Khan

A Thesis Submitted to
the Faculty of The Graduate School at
The University of North Carolina at Greensboro
in Partial Fulfillment
of the Requirements for the Degree
Master of Science

Greensboro
2018

Approved by

_____
Committee Chair

APPROVAL PAGE

This thesis written by Safeera Khan has been approved by the following committee of the Faculty of The Graduate School at The University of North Carolina at Greensboro.

Committee Chair _____
Zhenquan Jia

Committee Members _____
Paul Steimle

_____
Norman Chiu

_____
Jianjun Wei

_____
Date of Acceptance by Committee

_____
Date of Final Oral Examination

ACKNOWLEDGEMENTS

I would like to thank my advisor Dr. Zhenquan Jia for this opportunity and all Jia lab members. I also thank my committee members, Dr. Paul Steimle, Dr. Norman Chiu, and Dr. Jianjun Wei for their contributions and guidance. I thank my family and the Biology Department at the University of North Carolina at Greensboro for their help and support

TABLE OF CONTENTS

Page

LIST OF FIGURES

Page

CHAPTER I

INTRODUCTION

The prevalence of cardiovascular disease (CVD) and its impact on global health have been a cause of intense concern and research. The accumulation of plaque within arterial walls causes the diameter of the arterial lumen to decrease and restrict blood flow rate and volume. This condition is termed atherosclerosis and can lead to major cardiac and neural pathologies. Clinical manifestations of CVD can be in the form of myocardial infarction (MI), peripheral arterial disease, ischemic heart disease and stroke [2]. CVD presents an overwhelming economic and public welfare challenge, as it causes 30% of all deaths worldwide. Medicaid database results show CVD treatment is more expensive than diabetes, anxiety, and hypertension. In fact, one American dies every 36 seconds from some form of CVD [3].

As the demographics of Americans in terms of obesity rates and average age are increasing, the preventive and therapeutic treatment of CVD is at its most crucial point. One of the challenges of developing novel or improved methods for treatment or prevention of CVD is to identify the exact mechanism of development. One of the causative factors of CVD is reactive oxygen species (ROS), which can hasten dysfunction and cause downstream effects [4]. Thus, it is essential to identify the point at which controlling pathogenic ROS can halt or even reverse the progression of atherosclerosis.

Oxidative Stress and Atherosclerosis

Given the numerous complex mechanisms behind atherosclerosis, excess production of ROS has been shown to be one of the key contributing factors to its progression. ROS can be radicals, as in the case of the hydroxyl radical (·OH) or superoxide ($\cdot O^{2-}$). Others can be oxidizers, such as hydrogen peroxide (H_2O_2) and peroxynitrite ($ONOO^-$) [5, 6]. At low concentrations, ROS play a key role in helping endocrine balance, neuronal firing, enzyme activity and ion exchange. In fact, genetic defects that lead to limited ROS production are deleterious when dealing with pathogens as part of the innate immune response. Mitochondrial ROS are also involved in toll-like receptor (TLR) action which is used by sentinel immune cells [7]. H_2O_2 at low concentrations is used as a signaling molecule due to its longer half-life and ability to diffuse across membranes. Thus, ROS are essential components of cells and help to signal pathways throughout the body. However, overproduction of ROS disrupts homeostasis, causing endothelial inflammation and development of plaque.

The extreme chemical reactivity of ROS can cause damage to cellular macromolecules, membranes, and organelles. This occurs in abundance in blood vessels, which have high mitochondrial activity due to the continuous action of the heart [5]. Oxidative stress can occur at this point, which has many implications for cell viability and function. ROS overproduction is not just causative of CVD but also insulin resistance, obesity and metabolic syndrome [7]. The production of ROS is in large part due to the mitochondrial electron transport chain (ETC), xanthine oxidase, myeloperoxidase (MPO), nitric oxide synthase (NOS), lipoxygenase and nicotinamide

adenine dinucleotide phosphate oxidase (Nox). Nox reduce oxygen to form $O_2^{\bullet-}$ that are utilized by monocytes and neutrophils against pathogens [2]. Within the ETC, 2-3% of electrons are leaked and cause the formation of $O_2^{\bullet-}$. Many other cardiac cells such as vascular endothelial cells and cardiomyocytes express Nox variants that produce pathogenic and regulatory ROS. Thus, cardiovascular cells are highly susceptible to oxidative stress due to their level of activity and capability of overproducing ROS.

Firstly, some of the proteins producing superoxide radicals ($O_2^{\bullet-}$) are Nox types 1,2 and 5, which are known inducers of apoptosis in ECs [5]. Hypertension and angiotensin II receptor activity can lead to these forms of Nox overexpressing themselves, which further damages the vasculature. ApoE -/- mice without Nox2 showed a decrease in lesions, aortic ROS production, further confirming that inhibition of this isoform can be beneficial [8, 9]. In humans, Nox5 abundance and expression are heightened in coronary arteries with plaque buildup [7]. Secondly, endothelial NOS enzymes (eNOS) are abundant in the cardiovascular system, and they are heavily involved in ROS production. They facilitate electron transfer and convert L-arginine to L-citrulline. Uncoupling of eNOS from the electrons flowing through can cause reduction of molecular oxygen. Clinical studied in patients with diabetes and atherosclerosis showed increased eNOS uncoupling, leading to the production of $O_2^{\bullet-}$ [2]. In addition to this, genetic and environmental factors can also lead to increased ROS generation. For instance, studies on apolipoprotein E knockout (ApoE -/-) mice showed increased eNOS expression, atherosclerotic lesions, and $O_2^{\bullet-}$ generation [10].

Oxidized LDL: A Biomarker of Inflammation

ROS can oxidize low-density lipoproteins (LDL) and induce the formation of foam cells, which is the preliminary step to the development of plaque [11, 12]. The increase in ROS leads to EC dysfunction and vascular smooth muscle cell (SMC) proliferation and migration, both of which augment atherogenesis. LDL distribution in organs and time spent in circulation is governed by its size, which also influences cell-mediated endocytosis [13]. The oxidation of LDL (ox-LDL) is a well-established preliminary step of atherosclerosis, indicating its position as a risk factor for CVD. In healthy patients, CVD can be predicted by measuring ox-LDL levels, which further underscores their role as biomarkers of atherosclerosis. The protein moiety in LDL has been stained using immunohistochemistry, and results showed high concentration in atherosclerotic plaques [14]. LDL detaches from its transport vehicle in circulation and enters the arterial wall, where it comes in contact with oxidants from ECs. Transition metal ions or other catalysts can oxidize LDL, which leads to the inflammatory cascade and a positive feedback loop to make more ox-LDL [2, 15].

The progress of pre-atherosclerotic activity and its relation to ox-LDL is explained by macrophage uptake. These scavengers form foam cells that have abundant cholesteryl ester and cause EC dysfunction due to receptor-mediated ox-LDL uptake. The immune response against ox-LDL produces autoantibodies, which are elevated in the presence of atherosclerosis. It also increases the expression inflammatory cytokines, chemokines, and adhesion molecules in EC and monocytes. When ROS pose a threat to endothelial and underlying cells, these WBCs are guided to the site of inflammation. The

expression of inflammatory chemokines and cytokines like interleukin-8 (IL-8) and monocyte chemoattractant protein 1 (MCP-1/CCL2) further promotes leukocyte extravasation [16-19]. WBCs are also attracted by intracellular adhesion molecules (ICAM), VCAM, P-selectin and E-selectin [20]. The expression of these known inflammatory markers such as MCP-1 and VCAM-1 is induced in endothelial cells by the overproduction of ROS.

The lipids in highly ox-LDL become pro-apoptotic and cytotoxic as they develop in the intima-media [15]. Maturing atherosclerotic lesions have a lipid interior and a fibrous cap, which is weakened by necrosis and other events within the blood vessels. Apoptotic macrophages undergo autophagy but failed to carry out this process releases Nox and ROS, which expedites plaque rupture [7]. The rupture causes thrombosis, abruptly stopping blood and leading to MI or other forms of cardiac damage. The extracellular matrix around these cells can also be modified during ROS exposure, with increased leukocyte extravasation and remodeling via matrix metalloproteinases (MMPs) [5].

The Need for Improvement in Anti-Inflammatory Pharmacotherapy

Decades of laboratory and clinical trials have created therapies to treat and prevent ROS-mediated CVD. Antioxidants have been used to prevent ROS buildup and impede the inflammatory cascade. Lane et al. demonstrated the use of Vitamins A, C, and E lowers arterial dysfunction leading to disease. [5] It is important to note that antioxidant therapy has been largely unsuccessful in clinical trials. While ROS are important in CVD pathology, there are beneficial ROS that antioxidant therapy targets

without treating the underlying mechanism [20]. Thus, antioxidant therapy fails to be the pharmaceutical solution to treatment and prevention of CVD.

Some of the major classes of drugs used to ameliorate multiple effects of CVD are statins and angiotensin-converting-enzyme (ACE) inhibitors. Statins induce endothelial nitric oxide synthase (eNOS) action to indirectly combat EC damage and plaque formation [21]. Angiotensin II type I receptor blockers (ARBs) an also play a synergistic role in combating oxidative stress by decreasing carotid artery wall thickness and the amount of oxidative stress. Aspirin is also used in preventative ways to reduce MI risk, but its effect on stroke and CVD has not been conclusive [22]. However, they are debated in terms of use and side effects in high-risk populations.

The aforementioned drugs are not without their short- and long-term side effects, which calls for a moderated and individualistic approach by healthcare professionals [23]. The limitations of these therapies are short half-life in vivo, restricted bioavailability, and inability to permeate some biological membranes. Due to ROS-induced inflammation and its role in the progression of atherosclerosis, steroidal and non-steroidal anti-inflammatory drugs have been used to combat the inflammatory cascade. Thus, the side effects of these drugs create a need for better anti-inflammatory pharmacotherapy. This demand is leading the way for innovation in the form of nanomedicine, which can extend the boundaries of traditional pharmacotherapies and be a significant positive impact on the lives of atherosclerotic patients.

Nanomaterials in Oncologic and Cardiovascular Treatment

Nanomedicine provides new opportunities in the ongoing battle against reducing the health and economic damage caused by CVD. Nanotechnology allows the application of engineering to biological systems, which can create multi-disciplinary solutions to pathologies. The inherent properties of nanoparticles can be used for imaging and therapy for a variety of disorders that characterize CVD. Their chemical stability allows their interaction with membranes and fluids within the body, and their small size makes translocation possible [24-28].

Nanoparticles are distinct from macroscopic structures due to their sizes below 100 nm and unique physical, optical, mechanical and chemical properties. The properties of nanomaterials, such as structure, surface composition, and chemical reactivity dictate their effects in biological systems [13]. Surface passivation with homing ligands like monoclonal antibodies, peptides, or their mimetics can make targeting of specific biomarkers possible [29]. Poly(lactide-co-glycolide) (PLGA) nanoparticles in vivo caused a significant decrease in inflammatory monocyte subsets as compared to non-inflammatory monocytes, which shows their regulatory effects on the immune system [13]. Additionally, lipid-latex (LiLa) hybrid nanoparticles with phagocytic signals have been used to image and be vehicles in atherosclerotic models. These LiLa NPs were able to carry hydrophobic drugs and target inflammatory WBCs, while demonstrating steady drug release kinetics [30].

The multifaceted nature of NPs gives rise to a new ‘theranostic’ approach that combines the diagnostic capability of functionalized NPs with subsequent therapeutic

drug release. The events corresponding with plaque ruptures such as MMP upregulation, fibrous cap weakening, fibrin deposition, and macrophage concentration are all detectable by nano-theranostic means [31]. Nanoparticles have been successfully used for molecular imaging of plaque angiogenesis and lipoproteins [32]. The detection of CVD is equally challenging and essential due to the rapid reactivity of ROS with macromolecules. Traditional techniques are not able to fully detect the inflammatory process that leads to atherosclerotic lesions, and most fatal MIs are not detectable using x-ray angiography [33]. Nano-bioimaging can reveal where these reactions are taking place and detect their downstream effects. Although the proposed mechanism of LDL oxidation has been outlined, its exact location, progression, and cofactors have not been fully determined. For example, oxidized phospholipids (OxPL) in ox-LDL can be tracked and predict chances of MI, stroke, and other CVD-related deaths. Cell adhesion molecules are vital players in the inflammatory cascade, and nano-imaging techniques can reveal mechanisms of their action in real time. Thus, non-invasive imaging by NPs can enable early detection and preventative treatment of CVD [33].

Carbon Nanodots (CNDs): Applications in Nanomedicine

The medical applications of CNDs are highly dependent on their mechanism of interaction in the body. Semiconductor quantum dots (SQDs) were explored in this aspect due to their easy synthesis, optical properties, and photostability. However, their preparation required toxic metal ions and demonstrated oxidative degradation that challenged the safety of their use in biological systems [34]. SQDs can cause leaching of heavy metals and oxidation, which pose significant limitations in their medical use. There

have been attempts to reduce SQD toxicity by coating with polymers and hydrophilic chemicals, but there remains a need for economically produced and biocompatible nanoparticles.

Carbon nanodots (CNDs) are a novel addition to the family of nanomaterials, with exceptional biocompatibility, stability, fluorescence, and photoluminescence. The typical CND is < 10 nm and has a lattice spacing that resembles that of graphite with a chemical composition of carbon, oxygen, and surface functional groups. These functional groups help polarize the CND, making it hydrophilic and thus readily dispersible across most biological membranes. CNDs have an inner sp^2 and outer sp^3 hybridized structure that often has oxygen-containing functional groups. CNDs generally have a spherical shape, but varying synthetic methods can give crystalline structures [35].

The various methods of preparing CNDs can be classified broadly into a top down or bottom up syntheses. Top-down methods generally involve a larger carbon source being fragmented into increasingly smaller particles using hydrothermal or solvothermal cutting, laser ablation, chemical oxidation releasing or etching, and intercalation. Bottom-up approaches involve carbonization of organic precursors to synthesize CNDs. These can involve ultrasonication, solvent-mediated microwave pyrolysis and refluxing pyrolysis, as well as dehydration with sulfuric acid. Microwave pyrolysis reduces the reaction time, decreases side reactions, and increases the yield of CNDs [36]. The resulting product can undergo centrifugation, dialysis, chromatography, electrophoresis and other methods to give uniformity [37]. The morphology and structure of CNDs are heavily dependent on the precursor, method of preparation and experimental conditions.

The development of green synthetic methods of preparing CNDs was essential to improving their economic and environmental impact. Fluorescent CNDs have been prepared from various sources such as glucose, coffee grounds, ethylenediamine-tetraacetic acid (EDTA) salts, grass, soy milk and pomelo peels [38]. Hsu et al. were able to use a green-synthetic method to produce CNDs from coffee grounds. The grinding, heating, and separation process yielded the CNDs of diameter ~5 nm. FTIR analysis revealed surface caffeine, hydroxyl and carboxylate groups. The organic compounds in the coffee grounds provided hydrophilicity and passivation resulted in strong fluorescence [34]. The use of sweet potatoes to produce negatively charged CNDs was shown by Lu et al., which involved hydrothermal treatment of the complex carbohydrate. After reaching the point of supersaturation, burst nucleation resulted in fluorescent CNDs (1-3 nm) that could be used to detect Hg^{2+} [38]. Thus, green-synthetic CNDs were not only economical and relatively easy to produce, but they also had inherent properties that could be used to detect biologically active molecules.

The photoluminescent (PL) properties of gold, lead, silver and silicon nanodots have been used to detect DNA proteins and metal ions. Although some have shown high sensitivity, they have high economic and environmental costs, lower yield, and optical instability. The chemically inert nature, photostability and unique PL qualities give CNDs an advantage over Au nanodots, Ag nanoclusters, and SQDs [35]. The stability of CNDs can be observed by dissolving them in aqueous solutions and storing them at 4 °C. Green-synthesized CNDs stored in these conditions were stable for months without precipitating out of solution or detectable change in PL intensity [38]. Oil-based CNDs

underwent UV excitation for 6 months and storage for an additional 6 months and showed no observable PL intensity change [39]. The PL intensity of CNDs continuously exposed to laser irradiation did not decrease [35]. As demonstrated by Hsu et al., CNDs continuously excited for 6 h with a Xe lamp did not show a change in PL intensity [34]. The average absorbance of CNDs in the UV region is 330 – 420 nm is influenced by photon harvesting and has a tail in the visible region. However, π-π* bond and ketone group transition can cause CNDs to have a 250 – 300 nm band. Their emission wavelength is dependent on size and generally within 400 – 600 nm [34].

Green synthetic CNDs from coffee grounds were tested in LLC-PK1 cells to determine their internalization. Cell imaging revealed localization in the cytoplasm and cell membrane, possibly through endocytosis [34]. This demonstrated the ability of CNDs to remain stable and emit strong PL in culture media. 16HBE cells were treated with oil-based CNDs, and fluorescence imaging showed cytoplasmic localization after excitation at 488 nm. However, the nuclear region was devoid of any fluorescence, signaling that CNDs may not interact with or disrupt genetic material [39]. CA/CU-CNDs were observed in the membrane and cytoplasm of HeLa cells using multiphoton excitation fluorescence (MPEF) microscopy after a 24 hr incubation [40]. Thus, CNDs have been applied to biological systems in vitro and show their ability to cross membranes and thus interact with intracellular macromolecules.

There is currently no report on CND effects on the cardiovascular system, particularly its anti-oxidative potential in mediating ox-LDL induced EC dysfunction. ECs are central players in maintaining homeostatic balance and mediating pathogenic

processes in the cardiovascular system [7]. They determine the diameter, permeability and flow rate in blood vessels. In addition, they modulate growth and remodeling of vasculature and stem cells. As regulators of leukocyte extravasation during inflammation, ECs are key components of the development of atherosclerosis. The Human microvascular endothelial cell line 1 (HMEC-1) was isolated and immortalized in order to represent primary cultures for the investigation of CVD. HMEC-1s are well characterized and retain many of primary endothelial characteristics such as surface molecules. The expression of adhesion molecules (ICAM-1 and VCAM-1) on these cells are similar to those of human umbilical vein endothelial cells (HUVECs), a common model for endothelial cell research [41].

The morphological, phenotypical, and functional properties of primary HMECs are retained in HMEC-1, making it an accurate model for the mechanisms of endothelial dysfunction [42]. HMEC-1s also demonstrate receptor-mediated LDL particle uptake, which enables their use in the study of atherosclerosis. The primary goal of this study is to investigate the role of CNDs in the modulation of Ox-LDL-induced inflammation in HMEC-1 cells. Ox-LDL is a known biomarker of inflammation, and it affects the expression of genes involved with inflammatory response and leukocyte extravasation. I hypothesize that the antioxidant properties of CNDs can prevent ox-LDL-induced endothelial inflammation. Hence, this study examined the effects of CNDs on ox-LDL-induced endothelial cell dysfunction and their ability to ameliorate ox-LDL-mediated injury in HMEC-1s. The effect of CNDs on the health of C57BL/6 mice for 1 and 2 weeks was evaluated according to body weight and histology. The elucidation of CND

impact on ECs can provide additional information on the potential application of these nanoparticles for the treatment of inflammatory disorders leading to atherosclerosis.

CHAPTER II

MATERIALS AND METHODS

Cell Culture

HMEC-1 (ATCC® CRL-3243™) cells were grown in MCDB131 base medium without L-Glutamine. This was supplemented with 10 ng/mL Epidermal Growth Factor (EGF), 1 μg/mL Hydrocortisone, 10 mM Glutamine and a final concentration of 10% Fetal Bovine Serum (FBS). THP-1 cells were grown in RPMI-1640 medium supplemented with 10% FBS and 1% Pen-Strep. All cells were grown in Cellstar® Filter cap 75 cm^2 cell-culture treated filter screw cap flasks in humidified incubators at 37 °C and 5% CO_2. Respective media was renewed every 2 days, and cells were split into a new passage at 85% confluence.

CND Synthesis

Wendi Zhang (JSNN) synthesized CNDs by a microwave-assisted method using citric acid (0.96 g, 99%, ACROS Organics), 1.0 mL ethylenediamine (99%, Alfa Aesar) and 1.0 mL deionized H_2O. This solution was mixed in a glass vial and heated in a microwave synthesizer (CEM Corp 908005) at 300 W for 18 minutes. The resulting solution was then dialyzed against DI-H_2O (1000 MWCO, Fisher Scientific) for 24 hours. Then, a freeze-dryer (FreeZone 6, Labconco) was used to dry the solution, which gave the final solid product.

CND Characterization

UV-Vis spectroscopy was carried out using the Cary® Eclipse TM Fluorescence Spectrophotometer. CNDs were diluted to a concentration of 2 mg/mL in DI-H_2O and measured for fluorescence in a quartz cuvette. CNDS were excited at a wavelength of 350 nm. Then, they were excited at wavelengths 300 – 400 nm at 20 nm increments and measured for emission. Fourier transform infrared spectroscopy (FTIR) was used by Wendi Zhang to study the chemical structure and elemental content of CNDs.

Oxidation of LDL

Human Low-density lipoprotein (LDL) (99%) at 5mg/ml in 0.05M TRIS-HCl buffer, with 0.15M NaCl and 0.3mM EDTA, and pH 7.4 was purchased from Alfa Aesar. The LDL was dialyzed against phosphate buffer for 24 hours at 4 °C to remove buffer salts and macromolecules greater than 2,000 Daltons. After the addition of 10 mM $CuSO_4$, it was then incubated at 37 °C for 12 hours and used immediately for treatment. Ox-LDL was diluted to 25 – 100 μg/mL in 5 mL HBSS and added to cells.

CND and Ox-LDL Treatments

CND treatments were time-dependent, dose-dependent, and with or without co-treatment of Ox-LDL. Time-dependent treatments were set up as 24, 12, 6 and 3 hours. Dose-dependent treatments were 1.2, 0.6, 0.3, 0.2, 0.1, 0.03, 0.003, and 0.0003 mg/mL CND. When treating with CNDs, cells were grown in 100 mm × 10 mm Corning® cell culture-treated Petri dishes in the same incubator conditions. The treatment medium for HMEC-1 was sterile, filtered Hank's Balanced Salt Solution (HBSS) with 16 g NaCl, 0.8

g KCl, 0.06 g KH_2PO_4, 2 g Glucose, 0.096 g Na_2HPO_4, 0.28 g $CaCl_2$, 0.7 g $NaHCO_3$ and 0.1 g $MgCl_2$ per 2 liters of nanopure H_2O at pH 7.4.

CND Uptake Assay

HMEC-1 cells were cultured in complete MCDB131 medium and treated with 0 – 0.3 mg/mL CNDs at 85% confluence. After incubation at 37 °C, 5% CO_2 for 6 hours, treatment medium was discarded. Cells were rinsed with PBS (pH 7.8) to remove any membrane-bound CNDs. Cells were collected and resuspended in 1 mL PBS (pH 7.4) and measured for fluorescence using the Bio-Tek® Synergy 2™ plate reader at 360/40 excitation and 460/40 emission.

Quantitative Real-Time Polymerase Chain Reaction (qRT-PCR)

Cells were cultured in respective medium in 100 mm × 10 mm Corning® cell culture-treated Petri dishes until 85% confluence and media were discarded. Fresh HBSS or medium containing CND and LDL concentrations as described previously was incubated for a predetermined amount of time. After the incubation period, cells were washed with 37 °C PBS and transferred to an RNase-free hood. TRIzol™ reagent was used to extract RNA from cells according to the ThermoFisher Scientific™ RNA isolation protocol. After dilution of RNA in 15 µL RNase-free diethylpyrocarbonate (DEPC)-treated water, the concentration was measured.

RNA concentration and purity were determined by Thermo Scientific™ Nanodrop 2000, a full-spectrum UV-Vis spectrophotometer. Concentrations were normalized to 500 ng/µL, and cDNA was synthesized via reverse transcription. This used 14.875 µL DEPC-treated water, 5 µL 5x First Strand Buffer, 1.25 µL deoxynucleotide

triphosphate (dNTP) solution, 1.25 µL Random Primers, 0.625 µL Moloney Murine Leukemia Virus Reverse Transcriptase (M-MLV RT) and 2 µL RNA per sample. The cDNA was synthesized in Applied Biosystems™ Veriti™ 96 Well Thermal Cycler.

The genes of interest were targeted using 5 µL DEPC-treated water, 2 µL each of 5 µM forward and reverse primers, 10 µL Power SYBR® Green PCR Master Mix and diluted cDNA (1:5). The target genes were IL-8, NQO1, and GCL-C with GAPDH serving as the housekeeping gene. The Applied Biosystems™ StepOnePlus™ Real-Time PCR System was run for 40 cycles at the following settings: 95 °C for 15 seconds, 58 °C for 1 minute, and 60 °C for 15 seconds. In order to quantify gene expression, the comparative threshold cycle (C_T) values were used.

IDT® Human Primer Sequences

The primer sequences used are listed as follows: GAPDH Forward: 5’ – AGA ACG GGA AGC TTG TCA TC – 3’, GAPDH Reverse 5’ – GGA GGC ATT GCT GAT GAT CT – 3’. IL-8 Forward: 5’ – CTC TGT GTG AAG GTG CAG TT – 3’, IL-8 Reverse: 5’ – AAA CTT CTC CAC AAC CCT CTG – 3’. NQO-1 Forward: 5’ – TTA CTA TGG GAT GGG GTC CA – 3’ , NQO-1 Reverse: 5’ – TCT CCC ATT TTT CAG GCA AC – 3’. GCL,C Forward: 5’ – ACC ATC ATC AAT GGG AAG GA – 3’, GCL,C Reverse: 5’ – GCG ATA AAC TCC CTC ATC CA – 3’.

Monocyte Adhesion Assay

HMEC-1 cells were grown to confluence in Corning® tissue-culture treated culture dishes D × H 35 mm × 10 mm and treated with CNDs, Ox-LDL, or both for 6 hours. Prior to the end of treatment, THP-1 cells were counted using a hematocytometer

to allow 7.3×10^5 cells per dish. Monocytes were centrifuged at 1,500 RPM for 6 minutes and resuspended in 0.5% FBS RPMI in a 25 cm^2 flask. Invitrogen™ Calcein, AM at a final concentration of 0.75 µM was added, and the flask was gently tapped to ensure dispersal. After incubation at 37 °C, 5% CO_2 for 1 hour, THP-1 cells were centrifuged 1,500 RPM for 6 minutes and resuspended in 0.5% FBS RPMI media.

Treatment from HMEC-1 cells was stopped, and calcein-labeled THP-1 monocytes were added to facilitate binding. After 1 hour of incubation, cells were rinsed with PBS to remove unbound monocytes and collected. Cells were then resuspended in 1 mL pH 7.4 PBS and spun 5,000 RPM for 5 minutes. The supernatant was decanted, and cells were resuspended in 1 mL PBS, after which they were transferred to a black, opaque 96 well plate. The Bio-Tek® Synergy 2™ plate reader was used to measure fluorescence at excitation 485 nm, emission 520 nm.

Antioxidant Enzyme Lysate

Cells were treated with CNDs using the methods described previously. After the incubation period, cells were washed with PBS at 37 °C and incubated for 2 minutes to remove any remaining media. After decanting the PBS, 1.5 mL of trypsin was added per 75 cm^2 of cell growth surface area. The cells were incubated at 37 °C for 2 minutes, and trypsin was neutralized by the addition of 1 mL FBS and 10 mL growth medium. The cell suspension was centrifuged for 10 minutes at 1,500 RPM. The resulting pellet was suspended in 1 mL phosphate buffered saline (PBS). After centrifugation at 5,000 RPM for 5 minutes, the resulting pellet was resuspended in 300 µL sterile KH_2PO_4/K_2HPO_4 tissue buffer with 2 mM EDTA. This solution was sonicated for 15-second intervals 4

times and centrifuged at 13,000 RPM for 5 minutes. The resulting supernatant was collected and immediately analyzed for proteins.

Total Protein Concentration

Total protein content was measured using 10 µL lysate and 790 µL Bio-Safe™ Coomassie Brilliant Blue G-250 stain. This mixture was vortexed and transferred to cuvettes for spectrophotometric analysis. Absorbance was measured at 595 nm using the Beckman-Coulter® DU800 spectrophotometer. This was compared to a 1.48 mg/mL Bovine Serum Albumin (BSA) standard to determine cellular protein concentration.

Glutathione (GSH) Assay

HMEC-1 cells were grown to confluence and exposed to CND concentrations previously discussed for 24 hours. The lysate was treated with meta-phosphoric acid and 0.1% sodium phosphate buffer at pH 8.0 for 10 minutes. The resulting solution was centrifuged at 13,000 rpm for 5 minutes. The supernatant was incubated with 0.1% sodium phosphate buffer and o-phthalaldehyde (OPT) for 15 minutes. The fluorescence intensity was measured by excitation at 350 nm and emission at 420 nm. To account for interference with CNDs, samples were prepared in the same manner without OPT and measured. The difference between OPT and non-OPT was used as the final reading, which was calculated according to a 5 µg/mL GSH standard curve.

Glutathione S-Transferase (GST) Assay

The reaction mixture for measuring GST activity was prepared using 10 mL 0.1 M phosphate buffer (pH 6.5), 30 mg BSA, 100 µL of 10 mM GSH, and 200 µL of 50 mM 1-chloro-2,4-dinitrobenzene (CDNB) in ethanol. Then, 15 µL of lysate was mixed

with 585 µL reaction mixture in a cuvette and immediately transferred to a spectrophotometer, which read absorbance at 340 nm every 30 seconds for 5 minutes. A blank cuvette with 15 µL tissue buffer and 585 µL reaction mixture was run with each sample set.

NAD(P)H Quinone Dehydrogenase 1 (NQO1)

The reaction mixture for detecting NQO1 activity was prepared with 12 mL of 50 mM Tris-HCL buffer (pH 7.5, 0.08% Triton X-100), 36 µL of 50 mM Nicotinamide adenine dinucleotide phosphate (NADPH) and 48 µL of Dichlorophenolindophenol (DCPIP). 4 µL of the lysate was added to 696 µL of this reaction mixture in a cuvette and analyzed by the Beckman-Coulter® DU800 spectrophotometer. The rate of DCPIP reduction reflected NQO1 activity, which was measured at an absorbance of 600 nm.

Electron Paramagnetic Resonance (EPR) Spectroscopy

Hydroxyl radicals (OH·) generated by the Fenton reaction were measured by spin trap 5,5 dimethylpyrroline-N-oxide (DMPO). The reaction was as follows: $Fe^{2+} + H_2O_2 \rightarrow Fe^{3+} + OH\cdot + OH^-$. Thus, 10 mM DMPO, 50 µM $FeSO_4$, 50 µM H_2O_2, with 0 – 0.3 mg/mL CNDs were combined in PBS and transferred to a capillary tube at a final volume of 100 µL. Superoxide anions ($\cdot O_2^-$) were generated by the Xanthine/xanthine oxidase system and used spin trap 5-(Diethylphosphono)-5-methyl-1-pyrroline N-Oxide (DEPMPO). Thus, 0.1 mM DTPA, 10 mM DEPMPO, 360 µM xanthine and 32 mU/mL Xanthine Oxidase, with 0 – 0.3 mg/mL CNDs were combined in a capillary tube at a final volume of 100 µL. The EPR spectra were recorded at 25 °C using the Bruker D-200 ER, IBM-Bruker spectrometer operating at X-band with a TM cavity and capillary cell. The

settings for this spectrometer were as follows: modulation frequency, 100 kHz; X-band microwave frequency, 9.5 GHz; microwave power, 20 mW; modulation amplitude, 1.0G(gauss); time constant, 160 s; scan time, 200 s; and receiver gain, 1×10^5.

MTT Assay

HMEC-1 cells were grown in clear 24-well Costar® cell-culture treated plates to 85% confluence in respective media. Then, the culture medium was decanted and replaced with 300 µL/well of treatment medium. After the incubation at 37 °C and 5% CO_2, the treatment was decanted, and 33 µL of 0.2 mg/mL (3-(4,5-Dimethylthiazol-2-yl)-2,5-Diphenyltetrazolium Bromide) (MTT) was added. After 2 more hours of incubation, the MTT-containing solution was decanted, and 200 µL of dimethyl sulfoxide (DMSO) was added. Then, the plate was covered with aluminum foil and put on a shaker for 15 minutes at low speed. After the formazan crystals had dissolved, absorbance was measured at 570 nm using the Bio-Tek® Synergy 2™ plate reader for quantification and analysis.

Animal Project (Protocol 16-004)

Male C57BL/6 mice were purchased from Jackson laboratory at 10 weeks of age, and 24 mice were put into two exposure groups. The first group of 12 mice was exposed to CNDs for 1 week and the second group was exposed for 2 weeks. Each major group had 3 sub-groups that received IP administration of CNDs. Each group received a daily intraperitoneal injection (IP), and all mice were weighed every 3 days. The control group of 6 mice received 100 µL sterile saline, and an experimental group of 6 mice received

2.5 mg/kg body weight of CND. IP injection used a 27-gauge needle (0.5 in, BD) per mouse.

Animal care involved bedding changes every Tuesday and Friday with full cage changes every other week. Animals were given food, and water ad libitum and all caretaking were done by the student(s) and Principal investigator. Animals in this project were not subjected to any undue stress, pain, or overt discomfort. After the last injection, mice were anesthetized using isoflurane and confirmation of sedation was performed by the absence of withdrawal reflexes. Cardiac puncture was performed under isoflurane anesthesia to collect blood for analysis. After cardiac puncture, the animals did not awaken and were euthanized by cervical dislocation. The histopathology of the liver and kidneys was carried out by hemoxylin and eosin staining, with samples processed by AML Laboratories, Inc.

CHAPTER III

RESULTS

Characterization of CNDs: UV-Vis and FTIR

The photoluminescent properties of CNDs can be seen in their excitation wavelength of ~370 nm and an emission peak at ~450 nm. At 350 nm, the n-π* transition of C=O moieties can be seen in the absorption feature (Fig. 1A). Furthermore, CNDs were excited with various wavelengths from 300 – 400 nm and showed a consistent emission peak at 450 nm (Fig. 1B). FTIR spectra show the presence of (O-H) and (N-H) groups by the presence of broad bands from 3100 – 3400 cm^{-1}. Signals at 690 cm^{-1}, 1375 cm^{-1}, and 1550 cm^{-1} are due to the presence of C–C, C=C, and C=O groups, respectively.

CND Uptake by Endothelial Cells

The entry of CNDs into endothelial cells was measured by an uptake assay that involved 6 hour and 12 hour treatments (Fig. 2A). HMEC-1 cells were treated with 0 – 0.3 mg/mL CNDs and showed a significant ($P < 0.05$) dose-dependent increase in cellular internalization at both time points (Fig. 2B). The intensity of fluorescence at 6 hours was greater compared to the 12 hour incubation.

Monocyte Adhesion Decreases in Response to CND Co-Treatment

Endothelial cells undergoing inflammatory response synthesize adhesion molecules that help bind and extravasate leukocytes to the site of inflammation. This assay involved HMEC-1 cells treated with Ox-LDL and measured their adhesion to calcein, AM-labeled THP-1 monocytes. HMEC-1 cells treated for 6 hours with Ox-LDL showed a significant increase ($P < 0.05$) in monocyte adhesion at 25 – 50 µg/mL Ox-LDL, and a significant decrease ($P < 0.05$) at 75 – 100 µg/mL Ox-LDL (Fig. 3A). Next, cells treated with CNDs alone for 6 hours showed a decrease at 0.03 mg/mL CND and no significant change at 0.1 – 0.3 mg/mL CNDs (Fig. 3B). Cells were then co-treated for 6 hours with 50 µg/mL Ox-LDL and 0 – 0.3 mg/mL CNDs and showed a significant decrease ($P < 0.05$) in monocyte adhesion compared to the Ox-LDL group. (Fig. 3C).

CNDs Decrease Ox-LDL Induced Expression of Cytokine Interleukin-8

Inflammatory markers such as the cytokine interleukin-8 (IL-8) recruit WBCs to the site of inflammation and facilitate atherosclerotic development. Since Ox-LDL is a known inducer of inflammation, HMEC-1 cells were treated for different time points from 3 – 24 hours with 100 µg/mL Ox-LDL and measured for relative expression IL-8. Results from qRT-PCR show IL-8 was induced significantly ($P < 0.05$) from 24 – 6 hours of treatment (Fig. 4A). The time point of 6 hours was selected according to HMEC-1 cells' response to IL-8 expression. Next, Ox-LDL from 25 – 100 µg/mL was applied to HMEC-1 for 6 hours and showed the highest significant ($P < 0.05$) expression of IL-8 at 25 µg/mL Ox-LDL (Fig. 4B). HMEC-1 cells treated for 6 hours with CNDs showed a significant decrease ($P < 0.05$) at 0.03 – 0.3 mg/mL CND treatment (Fig. 4C). Then, cells

co-treated with CNDs and 25 µg/mL Ox-LDL significantly decrease ($P < 0.05$) IL-8 expression compared to the Ox-LDL group (Fig. 4D).

CND Effect on Cell Viability in HMEC-1 Cells

The effect of CNDs on HMEC-1 cell viability was assessed using the MTT assay, which indicates mitochondrial function. HMEC-1 cells treated for 6 hours with the same concentrations showed a significant increase in cell viability at 0.3 mg/mL CND and no significant change otherwise ($P < 0.05$) (Fig. 5).

Phase II Antioxidative Enzyme Levels in Response to CND Treatment

The amount of oxidative or reductive stress within a cell is indicated by levels of key antioxidants such as glutathione (GSH), glutathione-S-transferase (GST) and NAD(P)H dehydrogenase (quinone)-1 (NQO1). HMEC-1 cells were incubated for 12 hours with 0 – 0.3 mg/mL CNDs and measured for levels of total protein and Phase II antioxidant enzyme activity. The concentration of GSH (nmol/mg Protein) did not change significantly ($P > 0.05$) in response to CND treatment (Fig. 6A). The activity of GST (Fig. 6B) and NQO1 (Fig. 6C) showed no significant change ($P < 0.05$) with CND concentrations from 0.03 – 0.3 mg/mL compared to the negative control.

In order to determine NQO1 and GSH levels in response to CNDs, qRT-PCR was used to measure relative gene expression in cells. HMEC-1 treated with 0 – 0.3 mg/mL CNDs for 6 hours showed no significant change ($P < 0.05$) in NQO1 levels (Fig. 7A). However, the expression of GCL-C at 6 hours post-treatment was decreased significantly ($P < 0.05$) from 0.03 – 0.2 mg/mL CNDs compared to the control (Fig. 7B).

The Ability of CNDs to Scavenge ROS as Measured by EPR

EPR was used to show the generation of ·OH radicals using the Fenton reaction (Fe^{2+}/H_2O_2). The addition of CNDs to the DMPO-hydroxyl radical spin adduct shows a significant dose-dependent increase ($P < 0.05$) in scavenging ability from 0.01 – 0.3 mg/mL CNDs (Fig. 8A). This is also demonstrated by the EPR spectra showing diminishing peaks with increasing doses of CNDs (Fig. 8B). The Xanthine/xanthine oxidase (XO) system was used to study the effect of CNDs on Superoxide-scavenging activities. The effects of CNDs can be seen in the decrease of DEPMPO-superoxide ($DEPMPO/O_2^-$) adduct signal intensity (Fig. 9A). The EPR spectrum signal heights show a significant decrease ($P < 0.05$) with CNDs (0.01 – 0.3 mg/mL CNDs) compared to Xan/XO superoxide signal intensity (Fig. 9B).

Cytoprotective Effects of CNDs in Ox-LDL Induced Toxicity

The MTT assay was used to analyze the effects of CNDs on cells that were treated with cytotoxic concentrations of Ox-LDL. HMEC-1 cells treated for 6 hours with Ox-LDL show a dose-dependent decrease ($P < 0.05$) in viability from 50 – 125 μg/mL Ox-LDL (Fig. 10A). Co-treatment with CNDs (0.03 – 0.3 mg/mL) and Ox-LDL (50 μg/mL) showed a significant increase ($P < 0.05$) in cell viability from 0.03 – 0.3 mg/mL CNDs compared to the Ox-LDL group (Fig. 10B). As demonstrated previously (Fig. 5) CNDs alone did not affect cell viability.

1 and 2 Week CND Exposure of C57BL/6 Mice

At 10 weeks, male C57BL/6 mice were administered 2.5 mg/kg body weight CNDs by intraperitoneal (IP) injection for one (Fig. 11A) and two weeks (Fig. 11B).

Their body weight was taken periodically throughout the duration of exposure showed no significant change ($P > 0.05$) compared to the control group, which was given 100 µL saline via IP injection. Histological analysis of the kidney and liver focused on identifying anomalies between control and experimental groups. The kidney cortex was examined mainly on renal tubules and corpuscle. Lobes of the liver were also analyzed for central veins and portal triads. All examined structures between control and experimental groups were morphologically similar without showing observable pathological changes (Fig. 12 & 13).

CHAPTER IV

DISCUSSION

Atherosclerotic development is mediated by the immune response, which regulates WBC rolling and adhesion to the site of inflammation. This process is directed by chemotactic molecules that guide WBCs and adhesion markers that allow binding to ECs leading to their dysfunction. Once monocytes are directed to the underlying inflammation, their uptake of Ox-LDL continues the process. Additionally, SMCs and ECs can oxidize LDL in the presence of low concentrations of transition metals. This accelerates the rate of uptake by monocytes and poses toxicity to ECs and fibroblasts [43]. It involves activation by redox signaling, which can cause loss of membrane integrity, death, and eventual entry into circulation. Thus, endothelial dysfunction influences the initiation and pathological development of atherosclerosis [44].

The American Heart Association has determined the optimal LDL level as < 100 mg/dL, and high level as above 190 mg/dL [45]. Ox-LDL is recognized as an autoantigen and elicits a strong, chronic inflammatory response via receptor-mediated uptake by macrophages [44]. There is an urgent need for effective therapy with minimal side effects that targets Ox-LDL generation and pathogenesis as it relates to the development of CVD. As demonstrated in multiple studies, CNDs are a new class of nanomaterials with properties that enable their use in biological systems. In this study, we demonstrate that

Ox-LDL significantly increases the binding of monocytes to ECs, a major preliminary step to atherosclerotic development [43]. The addition of CNDs (0.1 – 0.3 mg/mL) to ECs induced with Ox-LDL (50 μg/mL) decreases their adhesion to monocytes, demonstrating their anti-inflammatory properties. This implies CNDs can provide significant protection against Ox-LDL induced inflammation and resulting pathogenesis.

The expression of cellular molecules like VCAM-1 and ICAM-1 and secreted cytokines such as IL-8 are heavily involved in the regulation of binding, rolling adhesion, and extravasation of monocytes into the underlying vascular tissue [46]. The role of IL-8 in recruiting and activating monocytes during an inflammatory response is demonstrated by the prevention of neutrophil extravasation when IL-8 is neutralized [47]. Accordingly, IL-8 -/- mice were resistant to developing atherosclerotic plaque, which underscores the importance of this cytokine in regulating monocyte adhesion and activation [46]. The exposure of HMEC-1s to Ox-LDL (100 μg/mL) increases the relative gene expression of IL-8 in a time-dependent manner (Fig. 4A). CND treatment also significantly suppresses the Ox-LDL-induced expression of IL-8 (Fig. 4D), and this anti-inflammatory activity of CNDs is consistent with their subdual of monocyte adhesion (Fig. 2C).

This activity of CNDs suggests their role in decreasing inflammatory cytokine production and resulting decrease of monocyte adhesion, extravasation, and plaque development. The expression of other biomarkers known to play a vital role in EC dysfunction and inflammation such as chemokines (MCP-1), cytokines (IL-6) , and adhesion molecules (VCAM-1, ICAM-1) remains to be investigated in their response to CNDs [48-50].

The underlying mechanism of CND suppression of Ox-LDL induced inflammation was investigated intracellularly. Given the numerous complex mechanisms behind atherosclerosis, excess production of ROS has been shown to be one of the key contributing factors to its progression. ROS include superoxide, hydrogen peroxide, hydroxyl radical, and peroxynitrite. These species are known to cause oxidation of LDL, promoting uptake by macrophages and formation of foam cells [51-53]. Increase in ROS can also cause endothelial cell dysfunction and apoptosis, vascular smooth muscle cell (SMC) proliferation and migration leading to atherogenesis [51-53].

The deleterious effects of ROS are countered by the activity of Phase II antioxidant enzymes like superoxide dismutase (SOD), glutathione peroxidase (GPx), glutathione-S transferase (GST) and NAD(P)H Quinone Dehydrogenase-1 (NQO1). SOD isoforms convert H_2O_2 and superoxide radicals to oxygen. GPx prevents lipid peroxidation, decreases EC sensitivity to Ox-LDL and converts lipid peroxides and H_2O_2 to lipid alcohols and water. GSH is a tripeptide (L-γ-glutamyl-L-cysteinyl-glycine) and acts as a buffer to conserve cellular thiol-disulfide redox capacity. Cellular forms of GSH can get oxidized to form glutathione disulfide (GSSG) and further oxidized into sulfonates. After GSH is synthesized, it is used to transport xenobiotics through multiple organ systems [54]. GST catalyzes the addition of a thiol group from reduced GSH to organic compounds. Thus, their hydrophilicity increases and this facilitates the detoxification and excretion of xenobiotics [55].

NQO1 is a flavoprotein that uses NADH or NADPH to perform two-electron reduction of quinones and scavenge superoxide radicals. This process is mediated by the

Keap1/Nrf2/ARE pathway and reduces the amount of ROS generation via redox cycling [56]. It facilitates conjugation in Phase II reactions for stabilization of radicals and eventual excretion [57]. In the presence of high cholesterol, these antioxidant enzymes are overwhelmed by the production of ROS. The development of drugs has focused on lowering cholesterol levels and increasing NOS efficiency, but these methods do not act directly on superoxide radicals [45].

It was then investigated if the anti-inflammatory action of CNDs could be attributed to their modulation of cellular phase II antioxidant enzymes. Thus, HMEC-1s treated with CNDs (0.03 – 0.3 mg/mL) were analyzed in regards to the activity of GSH, GST, and NQO1. Resulting data showed that CNDs had no significant effect on the activity of these antioxidants in HMEC-1s. This suggests the suppression of EC dysfunction and inflammation by CNDs is not due to their upregulation of cellular antioxidant defense mechanisms.

The overproduction of ROS causes oxidative stress in cells, which is further accelerated by uptake and oxidation of LDL. This process leads to the uptake of Ox-LDL particles by macrophages and their development into foam cells that contribute to plaque development [51-53]. Thus, it was investigated if the anti-inflammatory effects of CNDs are due to their scavenging of superoxide and hydroxyl radicals, which are potent ROS species. To this goal, EPR was used with DMPO/DEPMPO-spin trapping to see the effect of CNDs in scavenging ·OH and O_2^- generated from the Fenton reaction and Xanthine Oxidase/Xanthine system, respectively.

The DMPO–OH· adduct was represented as EPR spectra that had peaks signifying the intensity of ·OH generation using the following reaction: $Fe^{2+} + H_2O_2 \rightarrow Fe^{3+} + OH\cdot + OH^-$ (Fig. 8A). The DEPMPO-OOH adduct was represented as spectra with peaks indicating the intensity of O_2^- radicals generated using the following reaction: Xan + Xo → uric acid + O_2^-. The results of EPR indicate that the scavenging ability of CNDs (0.003 – 0.3 mg/mL) on ·OH and O_2^- radicals increased in a dose-dependent manner. This implies CNDs have direct scavenging activity on ROS, which may explain their anti-inflammatory effects in vitro. However, there needs to be further investigation on the exact mechanism of how the ROS-scavenging activity of CNDs suppresses atherosclerotic development.

The excess generation of intracellular ROS and uptake of Ox-LDL are shown to activate transcription factor NF-κB. The addition of Ox-LDL to ECs causes binding to lectin-like ox-LDL receptor-1 (LOX-1) and activates NF-κB [58]. This transcription factor is sequestered in the cytoplasm and inhibited by proteins (IkBα) until activated by phosphorylation. After IkBα is degraded, the heterodimers of NF-κB (p50/65) allow NF-κB translocation to the nucleus and regulation of inflammatory gene transcription [59-61]. Further investigation is needed to examine if uptake of Ox-LDL by HMEC-1s promotes ROS production, resulting in inflammation and if CNDs can suppress NF-κB activation by scavenging ROS.

The cytoprotective effects of CNDs due to their scavenging of ROS was further analyzed in HMEC-1s treated with a cytotoxic concentration OxLDL (50 μg/mL). After LDL enters ECs, it encounters pro-oxidants that convert it to Ox-LDL, which then

stimulates more ROS production and subsequent toxicity. When the cellular antioxidant defense is overwhelmed, it leads to the activation of signaling cascades involving NF-κB, nuclear factor-like 2 (Nrf2)/Kelch-like-ECH-associated protein 1 (Keap 1), and phosphoinositide 3-kinase (PI3K)/Akt. These processes lead to the activation of apoptotic pathways through activation of cysteine-dependent aspartate-specific proteases (caspases) [62]. Previous studies showed that Ox-LDL toxicity in HMEC-1 cells involves calpain activation and ubiquitination of caspase 3. This pathway mediated by calpain directs proteolysis of cytoskeletal elements, causing apoptosis, the release of cellular ROS and downstream development of atherosclerosis [63].

The effects of CNDs on Ox-LDL-induced cytotoxicity were measured by the reduction of MTT by mitochondrial dehydrogenase and NADH. Due to the ROS scavenging activity of CNDs, it was investigated if the Ox-LDL induced apoptotic pathway in ECs could be decreased or prevented. Incubation of cells with Ox-LDL (0 – 125 μg/mL) caused a dose-dependent decline in HMEC-1 cell viability due to the previously reported pathway. However, CNDs (0.03 – 0.3 mg/mL) were able to increase cell viability from 50% in Ox-LDL treated cells to 70 – 80% in cotreated (0.03 – 0.3 mg/mL CND + 50 μg/mL Ox-LDL) cells, indicating a marked cytoprotective effect. These results suggest the mechanism for HMEC-1 cell death could be due to Ox-LDL mediated oxidative stress and underscore the ability of CNDs to ameliorate this effect due to their ROS scavenging ability.

As demonstrated by the MTT assay, CND treatment (0 – 1.2 mg/mL) in HMEC-1s for 6 hours did not show a decrease in cell viability (Fig. 5). In order to observe these

effects in vivo, an investigation was performed to study the response of male C57BL/6 mice (10 wk) to interperitoneal (IP) administration of CNDs for 1 and 2 weeks. Mice were administered 2.5 mg/kg body weight CNDs daily for the duration of each experiment and showed no significant change in their body weights compared to the control group. The histological analysis focused on two major organs involved in detoxification and excretion, the liver and kidney. The effect of CNDs on the renal system was evaluated due to the vital filtration functions performed by highly vascularized nephrons. The semi-permeable glomerulus and surrounding Bowman's capsule showed no morphological changes compared to control mice. Additionally, analysis of portal triads, central veins and sinusoids were performed due to the liver's central role in detoxification. Liver lobules of CND-injected mice and control mice were showed no morphological changes or signs of pathology (Fig.12 &13).

These results in vivo show consistency with previously reported properties of CNDs in terms of biocompatibility, hydrophilicity, low toxicity and dose-dependent inhibition of tumor proliferation [64]. The optical properties of CNDs demonstrate innate, excitation-wavelength independent fluorescent as demonstrated in their consistent emission peak at 450 nm. This property was used to demonstrate the concentration-dependent uptake of CNDs into HMEC-1 cells for 6 and 12 hours (Fig. 2A and B). Thus, the fluorescent nature of CNDs enables their potential for use in bio-imaging of various tissues, which can provide future insight to biodistribution in vivo [65-68].

CHAPTER V

SUMMARY

This study demonstrated that CNDs can significantly reduce Ox-LDL induced monocyte adhesion in HMEC-1s, which indicates their anti-inflammatory effect in EC dysfunction. The relative gene expression of cytokine IL-8 was reduced by the cotreatment of CNDs, which implies their action in mediating monocyte extravasation to the site of inflammation. The overproduction of ROS leads to a cascade of signaling events that disrupt oxidative balance, induce EC dysfunction, and lead to an inflammatory state. Thus, EPR spectroscopy and radical spin-trapping were used to demonstrate the superoxide and hydroxyl radical-scavenging ability of CNDs. This suggests the anti-inflammatory effects of CNDs seen in vitro are attributed to their direct scavenging of ROS. This also allowed CNDs to ameliorate the cytotoxicity posed to HMEC-1s by treatment of Ox-LDL and induction of apoptotic pathways. Furthermore, CNDs alone did not show signs of cytotoxicity in vitro or vivo as demonstrated by the MTT assay and C57BL/6 mice exposure, respectively. The exact cellular and anti-oxidative mechanism of CNDs remains to be investigated in future studies. The collective findings of this study provide evidence for the use of these novel CNDs against Ox-LDL mediated inflammation and resulting cardiovascular disease.

REFERENCES

1. Borges, L.S.R. and E.S. Resende, *Coronary Microvascular Dysfunction.* International Journal of Cardiovascular Sciences, 2015. **28**(2).

2. Sugamura, K. and J.F. Keaney, Jr., *Reactive oxygen species in cardiovascular disease.* Free Radic Biol Med, 2011. **51**(5): p. 978-92.

3. Tarride, J.-E., et al., *A review of the cost of cardiovascular disease.* Canadian Journal of Cardiology, 2009. **25**(6): p. e195-e202.

4. Graham, M.R., et al., *Changes in endothelial dysfunction and associated cardiovascular disease morbidity markers in GH-IGF axis pathology.* Am J Cardiovasc Drugs, 2009. **9**(6): p. 371-81.

5. Panth, N., K.R. Paudel, and K. Parajuli, *Reactive Oxygen Species: A Key Hallmark of Cardiovascular Disease.* Adv Med, 2016. **2016**: p. 9152732.

6. Homa, S.T., et al., *Reactive Oxygen Species (ROS) in human semen: determination of a reference range.* J Assist Reprod Genet, 2015. **32**(5): p. 757-64.

7. Chen, K. and J.F. Keaney, Jr., *Evolving concepts of oxidative stress and reactive oxygen species in cardiovascular disease.* Curr Atheroscler Rep, 2012. **14**(5): p. 476-83.

8. Chuang, K., et al., *An expanding role for apolipoprotein E in sepsis and inflammation.* Am J Surg, 2010. **200**(3): p. 391-7.

9. Tibolla, G., et al., *Increased atherosclerosis and vascular inflammation in APP transgenic mice with apolipoprotein E deficiency.* Atherosclerosis, 2010. **210**(1): p. 78-87.

10. Vasunilashorn, S., et al., *Apolipoprotein E is associated with blood lipids and inflammation in Taiwanese older adults.* Atherosclerosis, 2011. **219**(1): p. 349-5

11. Michael R. Graham, P.E., Non-Eleri Thomas, Bruce Davies, Julien S. Baker, *Changes in Endothelial Dysfunction and Associated Cardiovascular Disease Morbidity Markers in GH-IGF Axis Pathology.* American Journal of Cardiovascular Drugs, 2009. **9**(6): p. 11.

12. Barbosa, K.B., et al., *Relationship of oxidized low density lipoprotein with lipid profile and oxidative stress markers in healthy young adults: a translational study.* Lipids Health Dis, 2011. **10**: p. 61.

13. Goonewardena, S.N., *Approaching the asymptote: obstacles and opportunities for nanomedicine in cardiovascular disease.* Curr Atheroscler Rep, 2012. **14**(3): p. 247-53.

14. Hammad, S.M., et al., *Oxidized LDL immune complexes and oxidized LDL differentially affect the expression of genes involved with inflammation and survival in human U937 monocytic cells.* Atherosclerosis, 2009. **202**(2): p. 394-404

15. Yoshida, H. and R. Kisugi, *Mechanisms of LDL oxidation.* Clin Chim Acta, 2010. **411**(23-24): p. 1875-82

16. Xing, D., et al., *Endothelial cells overexpressing interleukin-8 receptors reduce inflammatory and neointimal responses to arterial injury.* Circulation, 2012. **125**(12): p. 1533-41.

17. Bar-Eli, M., *Role of interleukin-8 in tumor growth and metastasis of human melanoma.* Pathobiology, 1999. **67**(1): p. 12-8.

18. Qian, B.Z., et al., *CCL2 recruits inflammatory monocytes to facilitate breast-tumour metastasis.* Nature, 2011. **475**(7355): p. 222-5.

19. W. Scott Simonet, T.M.H., Hung Q. Nguyen, Lisa D. Trebasky, Dimitry M. Danilenko, Eugene S. Medlockt, *Long-term Impaired Neutrophil Migration in Mice Overexpressing Human Interleukin-8.* The American Society for Clinical Investigation, Inc. , 1994. **94**: p. 1310-1319.

20. Zhang, N., B.T. Andresen, and C. Zhang, *Inflammation and reactive oxygen species in cardiovascular disease.* World J Cardiol, 2010. **2**(12): p. 408-10.

21. Calkin, A.C., et al., *The HMG-CoA reductase inhibitor rosuvastatin and the angiotensin receptor antagonist candesartan attenuate atherosclerosis in an apolipoprotein E-deficient mouse model of diabetes via effects on advanced glycation, oxidative stress and inflammation.* Diabetologia, 2008. **51**(9): p. 1731-40.

22. Hennekens, C.H., Schneider, Wendy R., *The need for wider and appropriate utilization of aspirin and statins in the treatment and prevention of cardiovascular disease.* Cardiovascular Therapy, 2008. **6**(1): p. 95-107.

23. Hanson, M. and P. Gluckman, *Endothelial dysfunction and cardiovascular disease: the role of predictive adaptive responses.* Heart, 2005. **91**(7): p. 864-6.

24. Matoba, T., et al., *Nanoparticle-mediated drug delivery system for atherosclerotic cardiovascular disease.* J Cardiol, 2017. **70**(3): p. 206-211.

25. Rosenblat, M., N. Volkova, and M. Aviram, *Selective oxidative stress and cholesterol metabolism in lipid-metabolizing cell classes: Distinct regulatory roles for pro-oxidants and antioxidants.* Biofactors, 2015. **41**(4): p. 273-88.

26. Xu, Z.Q., et al., *Highly Photoluminescent Nitrogen-Doped Carbon Nanodots and Their Protective Effects against Oxidative Stress on Cells.* ACS Appl Mater Interfaces, 2015. **7**(51): p. 28346-52.

27. Zeng, Z., et al., *A fluorescence-electrochemical study of carbon nanodots (CNDs) in bio- and photoelectronic applications and energy gap investigation.* Phys Chem Chem Phys, 2017. **19**(30): p. 20101-20109.

28. Zhang, W., Z. Zeng, and J. Wei, *Electrochemical Study of DPPH Radical Scavenging for Evaluating the Antioxidant Capacity of Carbon Nanodots.* The Journal of Physical Chemistry C, 2017. **121**(34): p. 18635-18642.

29. Gregory M Lanza, P.M.W., Shelton D Caruthers, Michael S Hughes, Tillmann Cyrus, Jon N Marsh, Anne M Neubauer, Kathy C Partlow, Samuel A Wickline, *Nanomedicine opportunities for cardiovascular disease with perfluorocarbon nanoparticles.* Nanomedicine. **1**(3): p. 321-329.

30. Bagalkot, V., et al., *Hybrid nanoparticles improve targeting to inflammatory macrophages through phagocytic signals.* J Control Release, 2015. **217**: p. 243-55.

31. Wang, D., B. Lin, and H. Ai, *Theranostic nanoparticles for cancer and cardiovascular applications.* Pharm Res, 2014. **31**(6): p. 1390-406.

32. Mulder, W.J. and Z.A. Fayad, *Nanomedicine captures cardiovascular disease.* Arterioscler Thromb Vasc Biol, 2008. **28**(5): p. 801-2.

33. McAteer, M.A. and R.P. Choudhury, *Targeted molecular imaging of vascular inflammation in cardiovascular disease using nano- and micro-sized agents.* Vascul Pharmacol, 2013. **58**(1-2): p. 31-8.

34. Hsu, P.-C., et al., *Synthesis and analytical applications of photoluminescent carbon nanodots.* Green Chemistry, 2012. **14**(4).

35. Roy, P., et al., *Photoluminescent carbon nanodots: synthesis, physicochemical properties and analytical applications.* Materials Today, 2015. **18**(8): p. 447-458.

36. Cayuela, A., et al., *One-Step Synthesis and Characterization of N-Doped Carbon Nanodots for Sensing in Organic Media.* Anal Chem, 2016. **88**(6): p. 3178-85.

37. Kurdyukov, D.A., et al., *Template synthesis of monodisperse carbon nanodots.* Physics of the Solid State, 2016. **58**(12): p. 2545-2549.

38. Lu, W., et al., *Green synthesis of carbon nanodots as an effective fluorescent probe for sensitive and selective detection of mercury(II) ions.* Journal of Nanoparticle Research, 2012. **15**(1).

39. Chen, B., et al., *Large scale synthesis of photoluminescent carbon nanodots and their application for bioimaging.* Nanoscale, 2013. **5**(5): p. 1967-71.

40. Stefanakis, D., et al., *Synthesis of fluorescent carbon dots by a microwave heating process: structural characterization and cell imaging applications.* Journal of Nanoparticle Research, 2014. **16**(10).

41. Munoz-Vega, M., et al., *Characterization of immortalized human dermal microvascular endothelial cells (HMEC-1) for the study of HDL functionality.* Lipids Health Dis, 2018. **17**(1): p. 44.

42. Ades, E.W., et al., *HMEC-1: Establishment of an Immortalized Human Microvascular Endothelial Cell Line.* Journal of Investigative Dermatology, 1992. **99**(6): p. 683-690.

43. Kuzuya M., Y.K., Hayashi T, Funaki C, Naito M, Asai K, Kuzuya F., *Oxidation of low-density lipoprotein by copper and iron in phosphate buffer.* Biochim Biophys Acta, 1991. **2**(1084): p. 198-201.

44. Sitia, S., et al., *From endothelial dysfunction to atherosclerosis.* Autoimmun Rev, 2010. **9**(12): p. 830-4.

45. Phoebe A Stapleton, A.G.G., Milinda E James, Robert W Brock, Jefferson C Frisbee, *Hypercholesterolemia and microvascular dysfunction: interventional strategies.* Journal of Inflammation. **2**(54).

46. Gerszten, R.E., et al., *MCP-1 and IL-8 trigger firm adhesion of monocytes to vascular endothelium under flow conditions.* Nature, 1999. **398**(6729): p. 718-23.

47. Harada, A., et al., *Essential involvement of interleukin-8 (IL-8) in acute inflammation.* Journal of Leukocyte Biology, 1994. **56**(5): p. 559-564.

48. Hansson, G.K., *Immune and inflammatory mechanisms in the pathogenesis of atherosclerosis.* J Atheroscler Thromb, 1994. **1 Suppl 1**: p. S6-9.

49. Libby, P., P.M. Ridker, and A. Maseri, *Inflammation and atherosclerosis.* Circulation, 2002. **105**(9): p. 1135-43.

50. Mangge, H., et al., *Antioxidants, inflammation and cardiovascular disease.* World J Cardiol, 2014. **6**(6): p. 462-77.

51. Hansson, G.K., *Inflammation, atherosclerosis, and coronary artery disease.* N Engl J Med, 2005. **352**(16): p. 1685-95.

52. Ross, R., *Atherosclerosis--an inflammatory disease.* N Engl J Med, 1999. **340**(2): p. 115-26.

53. Steinberg, D., *Atherogenesis in perspective: hypercholesterolemia and inflammation as partners in crime.* Nat Med, 2002. **8**(11): p. 1211-7.

54. Sies, H., *Glutathione and its role in cellular functions.* Free Radical Biology & Medicine, 1999. **27**(9): p. 916-921.

55. Matthew C.J. Wilce, M.W.P., *Structure and Function of glutathione S-transferases.* Biochim Biophys Acta, 1993. **1205**: p. 1-18.

56. Dinkova-Kostova, A.T. and P. Talalay, *NAD(P)H:quinone acceptor oxidoreductase 1 (NQO1), a multifunctional antioxidant enzyme and exceptionally versatile cytoprotector.* Arch Biochem Biophys, 2010. **501**(1): p. 116-23.

57. Ross, D., et al., *NAD(P)H:quinone oxidoreductase 1 (NQO1): chemoprotection, bioactivation, gene regulation and genetic polymorphisms.* Chem Biol Interact, 2000. **129**(1-2): p. 77-97.

58. Luciano C., P.A.F., Garbin U., Davoli A., Tosetti M.L., Campagnola M., Rigoni A., Pastorino A.M., Cascio V.L., and Sawamura T., *Oxidized Low Density Lipoprotein (ox-LDL) Binding to ox-LDL Receptor-1 in Endothelial Cells Induces the Activation of NF-□B through an Increased Production of Intracellular Reactive Oxygen Species.* The Journal of Biological Chemistry, 2000. **275**(17): p. 12633-12638.

59. Read, M.A., et al., *NF-kappa B and I kappa B alpha: an inducible regulatory system in endothelial activation.* J Exp Med, 1994. **179**(2): p. 503-12.

60. Brown, K., et al., *Control of I kappa B-alpha proteolysis by site-specific, signal-induced phosphorylation.* Science, 1995. **267**(5203): p. 1485-8.

61. Ouchi, N., et al., *Adiponectin, an adipocyte-derived plasma protein, inhibits endothelial NF-kappaB signaling through a cAMP-dependent pathway.* Circulation, 2000. **102**(11): p. 1296-301.

62. Redza-Dutordoir, M. and D.A. Averill-Bates, *Activation of apoptosis signalling pathways by reactive oxygen species.* Biochim Biophys Acta, 2016. **1863**(12): p. 2977-2992.

63. M Isabella Pörn-Ares, T.C.S., Tommy Andersson, and Mikko P S Ares, *Oxidized low-density lipoprotein induces calpain-dependent cell death and ubiquitination of caspase 3 in HMEC-1 endothelial cells.* Biochem J., 2003. **374**.

64. Hsu, P.-C., et al., *Extremely high inhibition activity of photoluminescent carbon nanodots toward cancer cells.* Journal of Materials Chemistry B, 2013. **1**(13): p. 1774-1781.

65. Liu, H., et al., *Microwave-assisted synthesis of wavelength-tunable photoluminescent carbon nanodots and their potential applications.* ACS Appl Mater Interfaces, 2015. **7**(8): p. 4913-20.

66. Liu, J., et al., *One-step hydrothermal synthesis of photoluminescent carbon nanodots with selective antibacterial activity against Porphyromonas gingivalis.* Nanoscale, 2017. **9**(21): p. 7135-7142.

67. Park, S.Y., et al., *Photoluminescent green carbon nanodots from food-waste-derived sources: large-scale synthesis, properties, and biomedical applications.* ACS Appl Mater Interfaces, 2014. **6**(5): p. 3365-70.

68. Zhu, S., et al., *Highly photoluminescent carbon dots for multicolor patterning, sensors, and bioimaging.* Angew Chem Int Ed Engl, 2013. **52**(14): p. 3953-7.

APPENDIX A

FIGURES

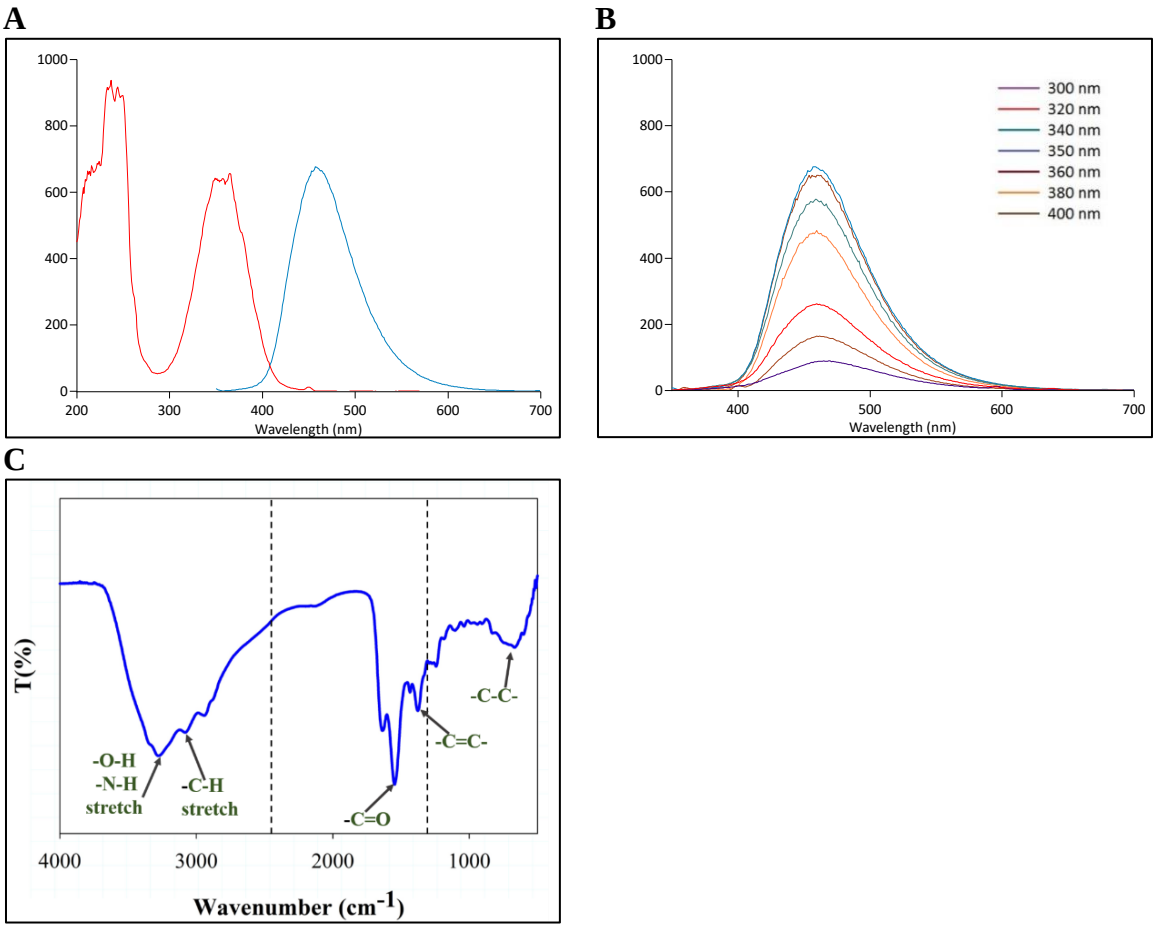

Figure 1. Characterization of CNDs. *UV-Vis photoluminescence in a.u. Measured by Cary®Eclipse TM Fluorescence Spectrophotometer. (a) Two excitation peaks are seen at ~220 nm and ~370 nm, and emission peak is ~450 nm. (b) CNDs show emission peak of ~450 nm with excitation wavelengths from 300 – 400 nm. (c) FTIR spectra indicate (O-H) and (N-H) groups by the presence of broad bands from 3100 – 3400 cm^{-1}. Signals at 690 cm^{-1}, 1375 cm^{-1}, and 1550 cm^{-1} are attributed to C–C, C=C, and C=O groups, respectively.*

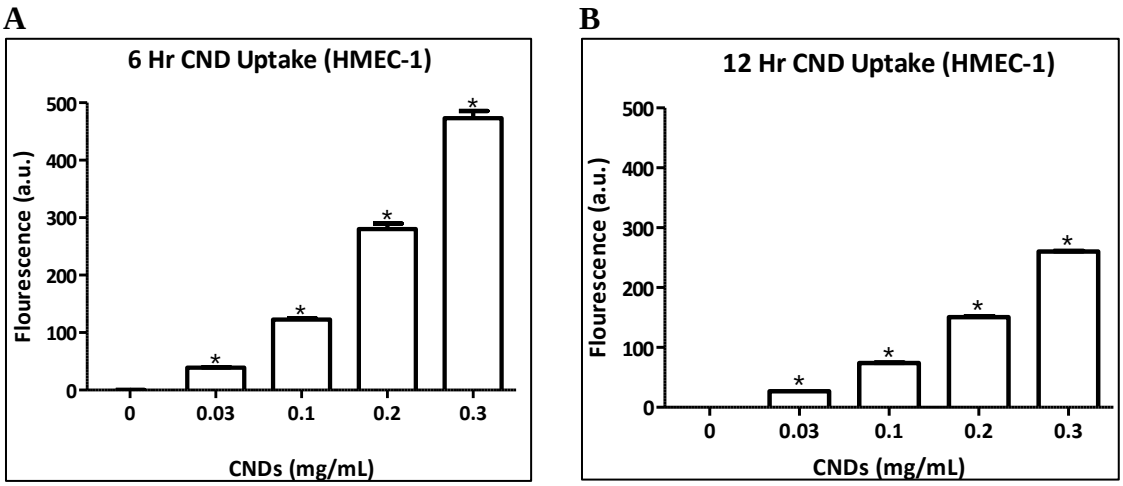

Figure 2. CND Uptake by HMEC-1 Cells*. (a) Cells treated with 0 – 0.3 mg/mL CNDs in HBSS for 6 hours show a dose-dependent increase in fluorescence intensity. (b) Cells treated with 0 – 0.3 mg/mL CNDs in HBSS for 12 hours show a dose-dependent increase in fluorescence. All data represent mean ± SEM. (n = 5. *, P < 0.05 vs. control)*

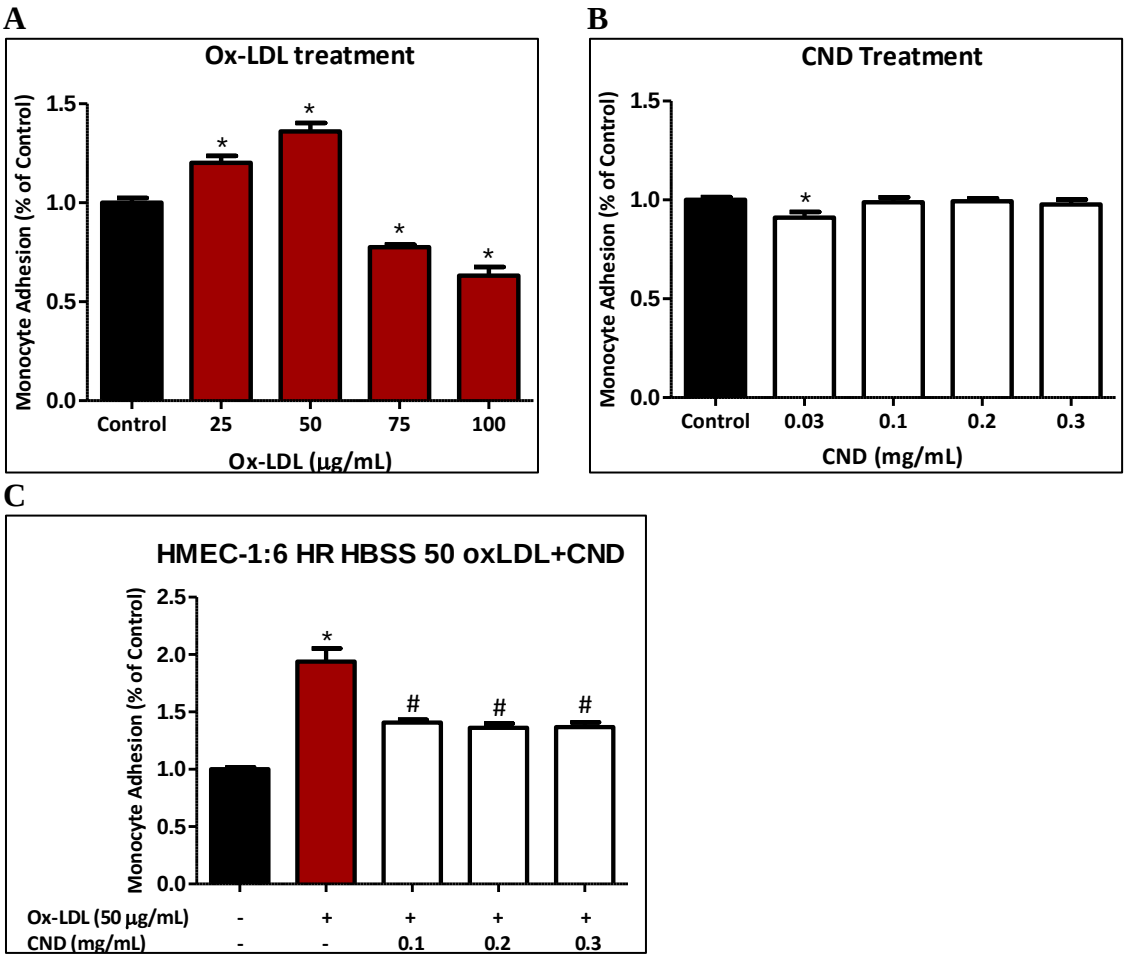

Figure 3. CNDs Inhibit Ox-LDL-Induced Monocyte Adhesion. *(a) HMEC-1 cells were treated with Ox-LDL for 6 hrs, and calcein-AM-labeled monocytes were co-incubated for 1 hr post-treatment. (b) Cells were treated with CNDs for 6 hrs and calcein-AM-labeled monocytes were co-incubated for 1 hr post-treatment. (c) HMEC-1 cells were co-treated with 50 ug/mL ox-LDL and 0.1 – 0.3 mg/mL CNDs for 6 hrs and calcein-AM-labeled monocytes were co-incubated for 1 hr post-treatment. All data represent mean ± SEM. (n = 3.*, P < 0.05 vs. control, #, P < 0.05 vs. Ox-LDL)*

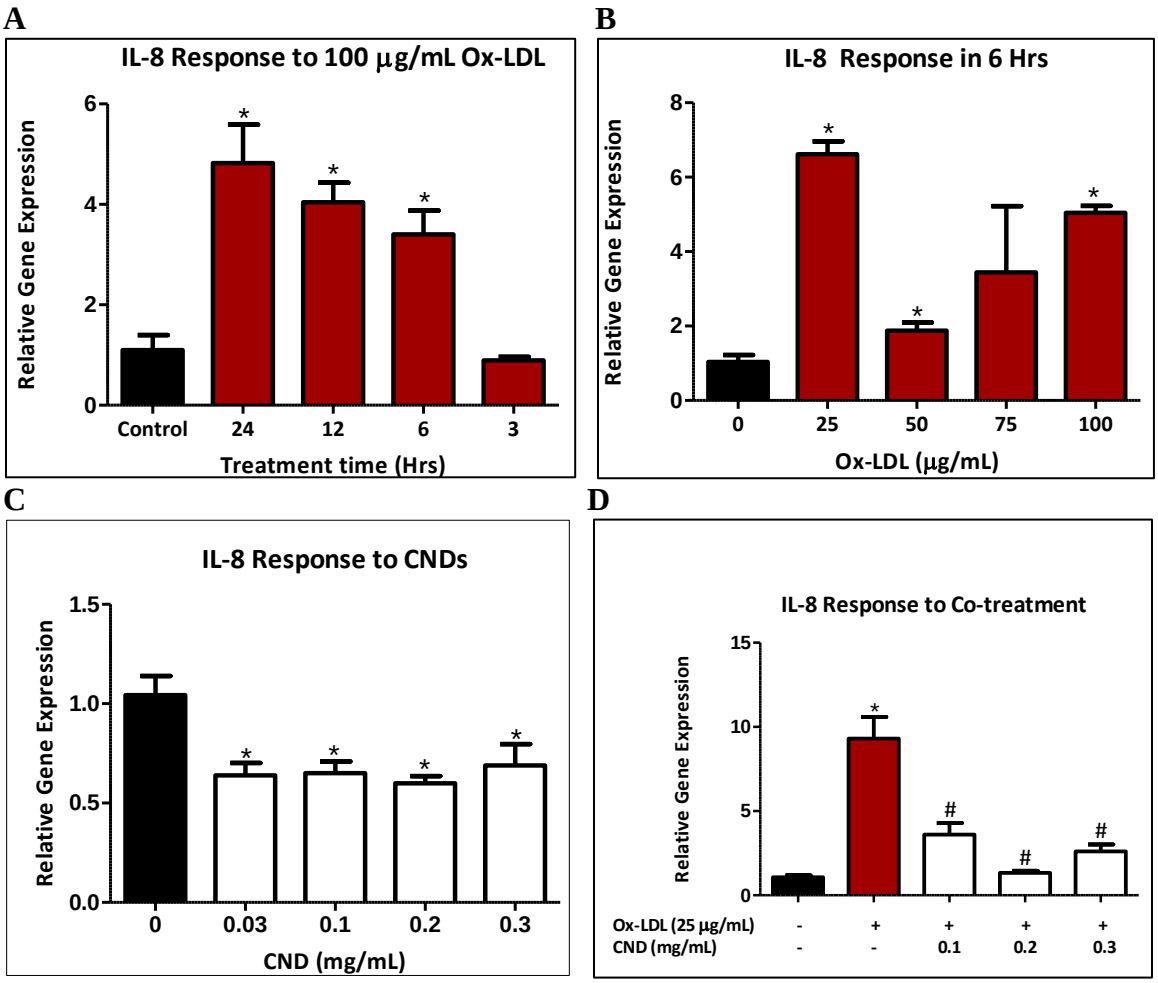

Figure 4. CNDs Decrease HMEC-1 Expression of IL-8 Induced by Ox-LDL. *(a) Cells treated with 100 ug/mL ox-LDL from 6 – 24 hrs (n = 3) (b) Cells treated with 0 – 100 ug/mL ox-LDL for 6 hrs (n = 3) (c) Cells treated with 0.03 – 0.3 mg/mL CNDs for 6 hours (n = 9) (d) HMEC-1 cells were cotreated 25 ug/mL ox-LDL and 0.1 – 0.3 mg/mL CNDs for 6 hrs, (n = 12), All data represent mean ± SEM. (*, P < 0.05 vs. control, #, P < 0.05 vs. Ox-LDL)*

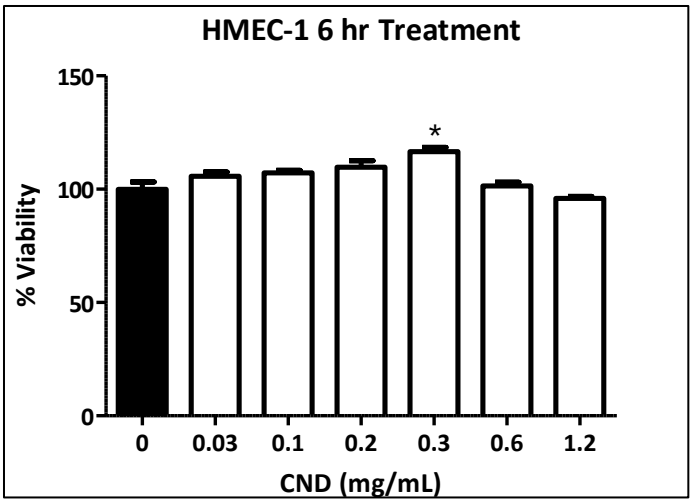

Figure 5. CND Effect on Cell Viability. *HMEC-1 treated with CNDs for 6 hours in HBSS show a significant increase in viability at 0.3 mg/mL. All data represent mean ± SEM. (n = 4,*, P < 0.05 vs. control)*

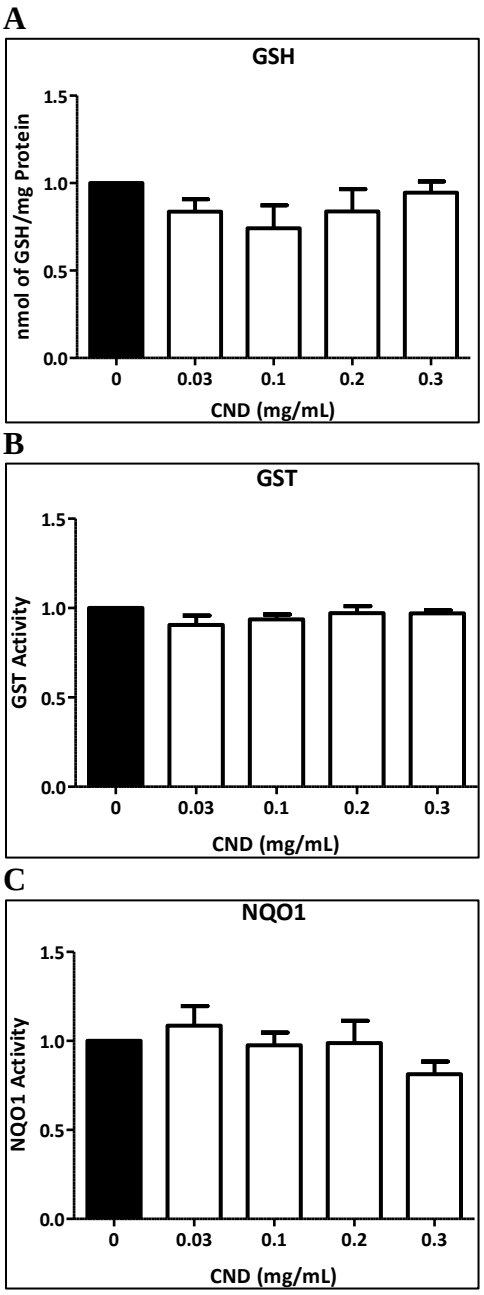

Figure 6. Effects of CND Treatment on Phase II Antioxidant Activity. *CNDs were incubated with HMEC-1 cells for 12 hours in HBSS, and total protein level was measured (a) There was no significant change in the amount of glutathione from 0 – 0.3 mg/mL CNDs. (b) There was no significant change in the activity of GST from 0 – 0.3 mg/mL CNDs. (c) There was no significant change in the amount of NQO-1 activity from 0 – 0.3 mg/mL CNDs. All data represent mean ± SEM (n = 4, P < 0.05 vs. control)*

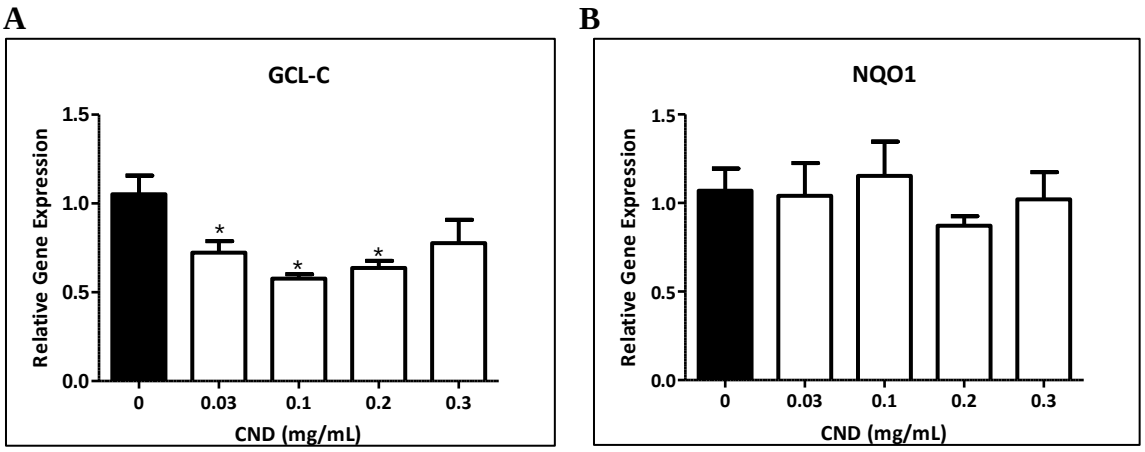

Figure 7. Effect of CNDs on the Expression of Phase II Antioxidant Genes *HMEC-1 treated with CNDs from 0.03 – 0.3 mg/mL CNDs for 6 hrs in HBSS. (a) There was no significant change in NQO1 expression (b) The expression of GCL-C was significantly decreased from 0.03 – 0.2 mg/mL CND. All data represent mean ± SEM (n = 12.*, P < 0.05 vs. control)*

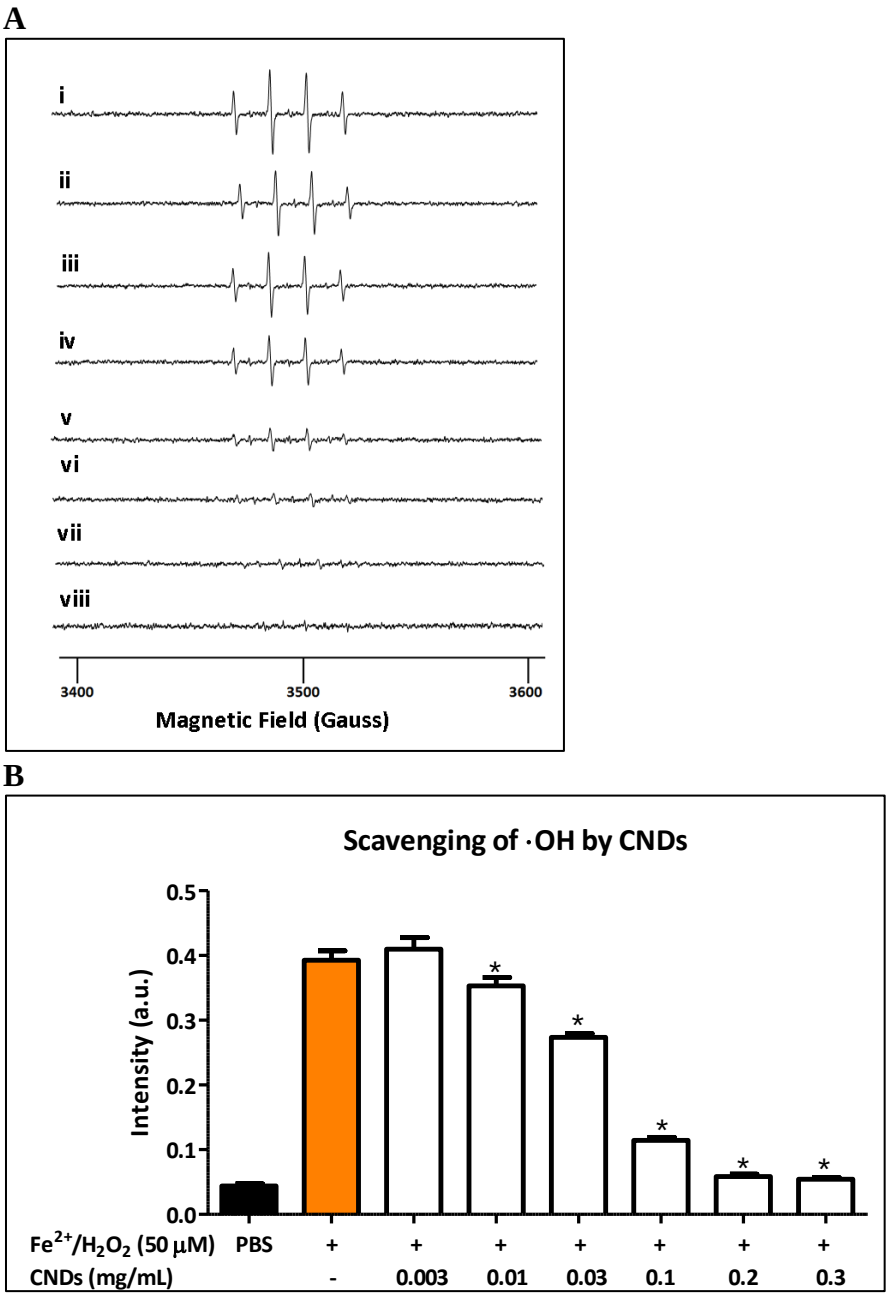

Figure 8. CND Scavenging Activity on Hydroxyl Radicals. *The reaction contained 50 µM $FeSO_4$ and 50 µM H_2O_2 (A) EPR spectra show (i) Fe^{2+}/H_2O_2 (50 µM) only. Fe^{2+}/H_2O_2 is in all reactions with the following additions of CNDs (mg/mL) (ii) + 0.003 (iii) + 0.01 (iv) + 0.03 (v) + 0.1 (vi) + 0.2 (vii) + 0.3 (viii) PBS only (B) Signal intensity at 3480 G. All data represent mean ± SEM , n = 3. Turkey's HSD post hoc test for each treatment showed differences ($P \leq 0.05$); *, significant differences compared to control*

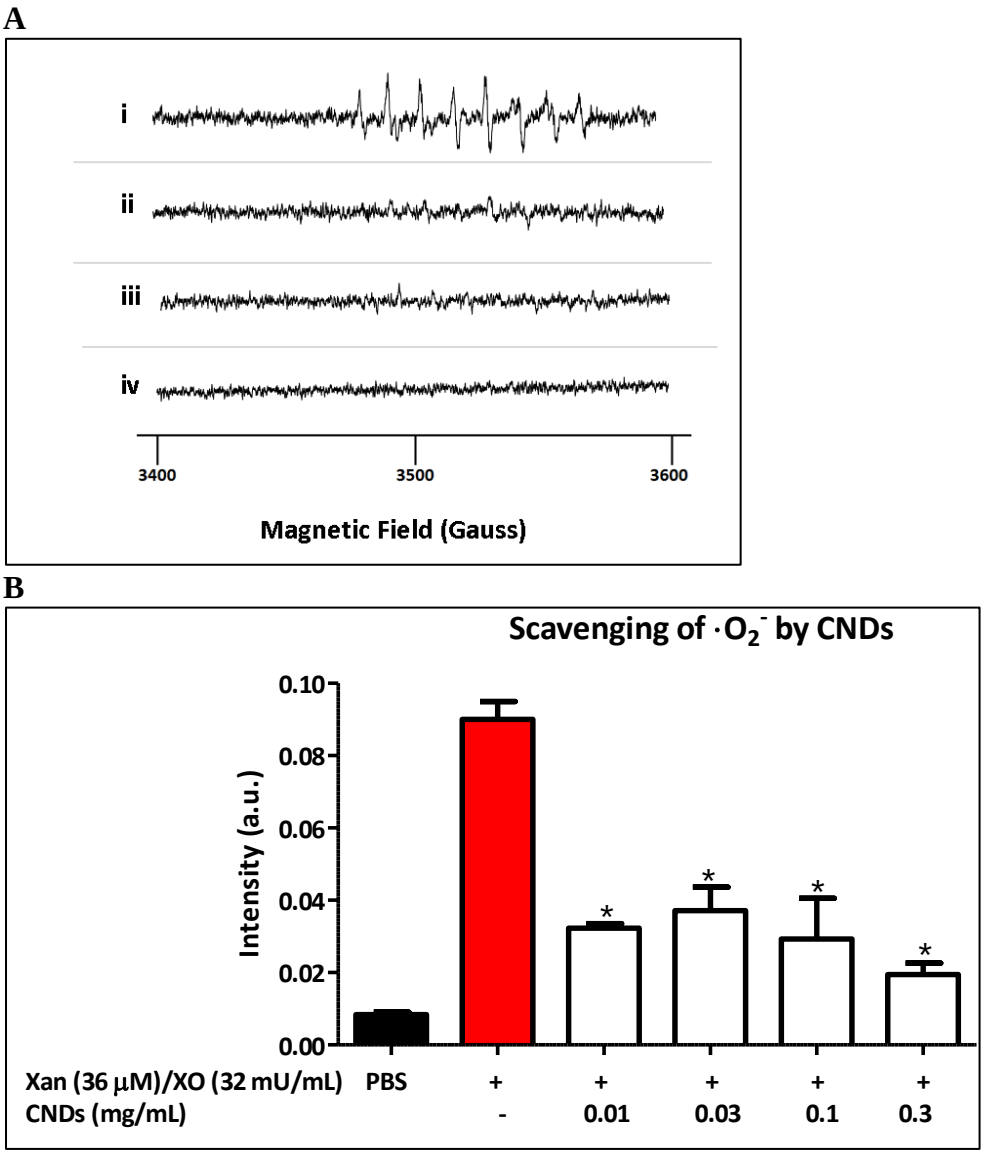

Figure 9. CND Scavenging Activities on Superoxide Radicals. The *reaction conditions and EPR settings were as described in Materials and Methods in the presence of 36 µM xanthine and 32 mU/ml xanthine oxidase. (A) EPR spectra of DEPMPO-superoxide spin adduct in the absence and presence of CNDs (ii) Xan/XO Superoxide generating system (ii) Xan/XO Superoxide generating system + 0.01 mg/mL CND (iii) + 0.03 mg/mL CND (iv) PBS only (B) Signal intensity at 3480 G. All data represent mean ± SEM , n = 3. Turkey's HSD post hoc test for each treatment showed differences ($P \leq 0.05$); *, significant differences compared to control*

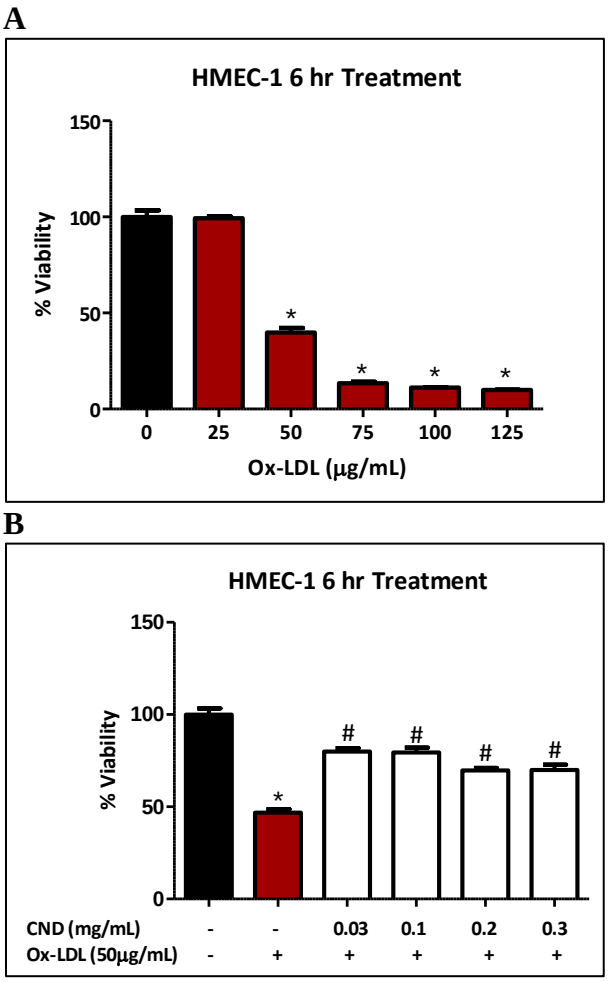

Figure 10. Cytoprotective Effects of CNDs Against Ox-LDL Induced Toxicity. *A: HMEC-1 were treated with 0 – 100 ug/mL ox-LDL for 6 hrs in HBSS B: HMEC-1 cells were cotreated with 50 ug/mL ox-LDL and 0.03 – 0.3 mg/mL for 6 hrs in HBSS. All data represent mean ± SEM (n = 4.*, P < 0.05 vs. control)*

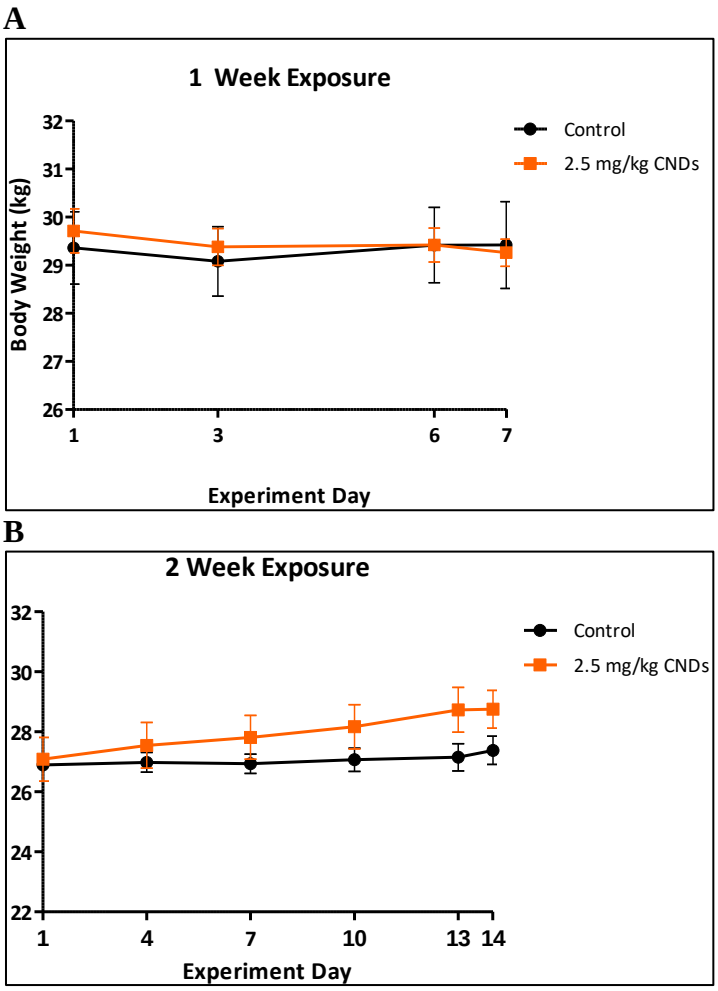

Figure 11. Mice Body Weights of 1 and 2 Week CND Exposure. *Mice interperitoneally injected with 2.5 mg/mL CNDs/kg bw daily for one week (A) or two weeks (B); Control mice injected with 100 µL saline. All data represent mean ± SEM (n = 6. P < 0.05)*

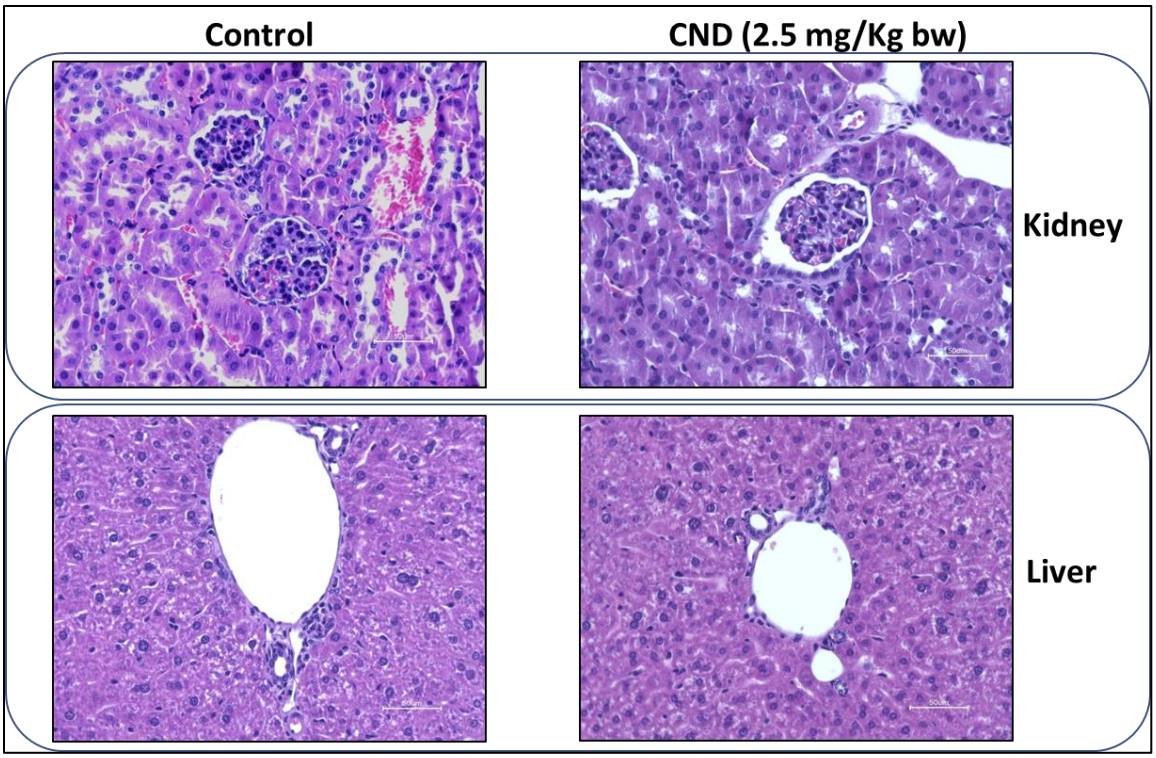

Figure 12. Week 1 CND Exposure Histology. *Mice interperitoneally injected with 2.5 mg/mL CNDs/kg bw daily for one week; Control mice injected with saline. A: Kidney B: Liver.*

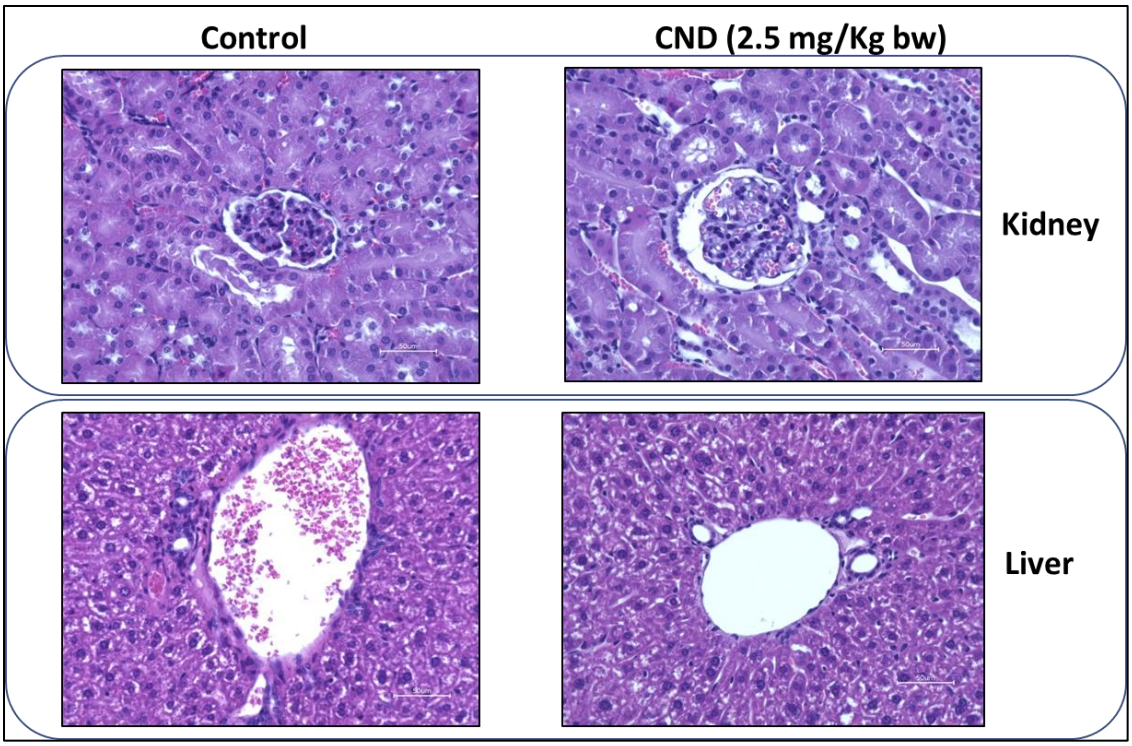

Figure 13. Week 2 CND Exposure Histology. *Mice interperitoneally injected with 2.5 mg/mL CNDs/kg bw daily for two weeks; Control mice injected with saline. A: Kidney B: Liver.*